Elsevier Editorial System(tm) for Geomorphology
Manuscript Draft

Manuscript Number: GEOMOR-2765R1

Title: LATE HOLOCENE EVOLUTION OF PLAYA LAKES IN THE CENTRAL EBRO DEPRESSION BASED ON GEOPHYSICAL SURVEYS AND MORPHO-STRATIGRAPHIC ANALYSIS OF LACUSTRINE TERRACES

Article Type: Special Issue: Geomorphology in Spain

Keywords: deflation basins, paleohydrology, trenching, geophysics, Holocene, saline lakes

Corresponding Author: Dr. Francisco Gutierrez,

Corresponding Author's Institution: Universidad de Zaragoza

First Author: Francisco Gutierrez

Order of Authors: Francisco Gutierrez

Abstract: The origin and morpho-stratigraphic evolution of the largest playa-lake system (La Playa-El Pueyo) in the Bujaraloz-Sástago endorheic area, located in the semiarid central sector of the Ebro Depression, are analysed. The enclosed depressions are developed on gypsiferous Tertiary bedrock and show a prevalent WNW-ESE orientation parallel to the direction of the prevalent strong local wind (Cierzo). Yardangs have been carved in bedrock and unconsolidated terrace deposits in the leeward sector of the largest lake basins. A sequence of three lacustrine terrace levels has been identified by detailed geomorphological mapping. The treads of the upper, middle and lower terrace levels are situated at +9 m, +6 m and +0.5 m above the playa-lake floors, respectively. Seismic refraction and electrical resistivity profiles acquired in La Playa reveal a thin basin fill (~2 m) with a planar base. These data allows ruling out the genetic hypothesis for the depressions involving the collapse of large bedrock cavities and supports a mixed genesis of combined widespread dissolution and subsidence by groundwater discharge and eolian deflation during dry periods. The 5 m thick deposit of the middle terrace was investigated in hand-dug and backhoe trenches. Six AMS radiocarbon ages from this terrace indicate an aggradation phase between 3.9 ka and ca. 2 ka. These numerical ages yield a maximum average aggradation rate of 2.6 mm/yr and a minimum excavation rate by wind deflation of 3 mm/yr subsequent to the accumulation of the middle terrace. The latter figure compares well with those calculated in several arid regions of the world using yardangs carved in paleolake deposits. The aggradation phase between 4-2 ka is coherent with other Iberian and Mediterranean records showing relatively more humid conditions after 4 ka, including the Iron Ages and the Iberian-Roman Period.

LATE HOLOCENE EVOLUTION OF PLAYA LAKES IN THE CENTRAL EBRO DEPRESSION BASED ON GEOPHYSICAL SURVEYS AND MORPHO-STRATIGRAPHIC ANALYSIS OF LACUSTRINE TERRACES

F. Gutiérrez (1*), B. Valero-Garcés (2), G. Desir (1), P. González-Sampériz (2), M. Gutiérrez (1), R. Linares (3), M. Zarroca (3), A. Moreno (2), P. Lucha (4), J. Guerrero (1), C. Roqué (5), L.J. Arnold (6), M. Demuro (6)

(1) Departamento de Ciencias de la Tierra, Universidad de Zaragoza, Zaragoza, Spain

(2) Pyrenean Institute of Ecology (CSIC), Zaragoza, Spain

(3) Àrea de Geodinàmica Externa i Hidrogeologia, Universitat Autònoma de Barcelona, Barcelona, Spain

(4) Colorado Geological Survey, Colorado, USA

(5) Àrea de Geodinàmica Externa i Geomorfologia, Universitat de Girona, Girona, Spain

(6) Centro Nacional de Investigación sobre la Evolución Humana (CENIEH), Burgos, Spain

* Corresponding autor e-mail: fgutier@unizar.es

Abstract

The origin and morpho-stratigraphic evolution of the largest playa-lake system (La Playa-El Pueyo) in the Bujaraloz-Sástago endorheic area, located in the semiarid central sector of the Ebro Depression, are analysed. The enclosed depressions are developed on gypsiferous Tertiary bedrock and show a prevalent WNW-ESE orientation parallel to the direction of the prevalent strong local wind (Cierzo). Yardangs have been carved in bedrock and unconsolidated terrace deposits in the leeward sector of the largest lake basins. A sequence of three lacustrine terrace levels has been identified by detailed geomorphological mapping. The treads of the upper, middle and lower terrace levels are situated at +9 m, +6 m and +0.5 m above the playa-lake floors, respectively. Seismic refraction and electrical resistivity profiles acquired in La Playa reveal a thin basin fill (~2 m) with a planar base. These data allows ruling out the genetic hypothesis for the depressions involving the collapse of large bedrock cavities and supports a mixed genesis of combined widespread dissolution and subsidence by groundwater discharge and eolian deflation during dry periods. The 5 m thick deposit of the middle terrace was investigated in hand-dug and backhoe trenches. Six AMS radiocarbon ages from this terrace indicate an aggradation phase between 3.9 ka and ca. 2 ka. These numerical ages yield a maximum average aggradation rate of 2.6 mm/yr and a minimum excavation rate by wind deflation of 3 mm/yr subsequent to the accumulation of the middle terrace. The latter figure compares well with those calculated in several arid regions of the world using yardangs carved in paleolake deposits. The aggradation phase between 4-2 ka is coherent with other Iberian and Mediterranean records showing relatively more humid conditions after 4 ka, including the Iron Ages and the Iberian-Roman Period.

Key words: deflation basins**,** paleohydrology, trenching, geophysics, Holocene, saline lakes

1. Introduction

The central sector of the Ebro Depression in NE Spain (Fig. 1) constitutes a particularly interesting and challenging area for paleoclimatic investigations due to several reasons: (1) It is the northernmost semiarid region in Europe, bounded by mountain ranges that were glaciated during the Quaternary. (2) Climate variability during the last glacial cycle may differ substantially from other European areas (Harrison et al., 1996; Prentice et al., 1998; Davis et al., 2003; Valero-Garcés et al., 2000a; González-Sampériz et al. 2008) due to the combined influence of both North Atlantic and sub-tropical climates (Summer et al., 2001). (3) Lacustrine records are largely restricted to saline lakes of poorly understood geomorphic origin and evolution, including the northernmost playa-lakes with active evaporite deposition in Europe. Studies focused on saline lake sediments provide evidence for a complex paleohydrological evolution over the last glacial cycle in the semiarid Ebro Depression, with several abrupt and rapid arid/humid transitions (Valero-Garcés et al., 1998; 2000a; González-Sampériz et al., 2008). However, the chronological control of most lake sequences is rather limited due to the scarcity of organic remains in the sediments and the presence of erosional hiati.

Holocene paleoenvironmental interpretations of the Ebro Depression are based mostly on cores drilled in saline lakes located in internally drained depressions: Mediana (Valero-Garcés et al., 2000a, c), Bujaraloz-Sástago (Pérez-Obiol and Roure, 1990; Stevenson et al., 1991; Davis, 1994; Schütt, 1998; Davis et al., 2003; Moreno et al., 2004; González-Sampériz et al., 2008; Mees et al., 2011), Chiprana (Davis, 1994; Valero-Garcés et al., 2000b), Alcañiz (Stevenson et al., 1991; Davis, 1994) and Hijar areas (Davis, 1994). In spite of the large efforts carried out to investigate their stratigraphic record from a paleoenvironmental perspective, the origin and morpho-

stratigraphic evolution of the enclosed basins remain unclear. The lack of data on the subsurface geometry of the basins precludes evaluating the validity of the different hypotheses proposed to explain the formation of the closed depressions in evaporitic bedrock. Additionally, reconstructing the evolution of these lacustrine basins requires taking into account the scarcely investigated terraces preserved at the lake margins.

As González-Sampériz et al. (2008) point out, stratigraphic records from the bottom of playa-lakes in the Ebro Depression pose significant limitations to paleoenvironmental studies: (1) Limited thickness and temporal length of the sequences. (2) Significant hiati attributable to enhanced wind erosion, difficult to identify in cores. (3) Very low pollen content and material datable by the radiocarbon method. (4) Significant diagenetic overprinting favoured by the continuous upward discharge of saline groundwater flows and the inherent instability of evaporitic minerals (Warren, 2006). (5) Reworking and contamination processes. (6) Limited preservation potential of biological indicators. Recently, detailed geomorphological mapping has revealed the presence of stepped sequences of aggradational lacustrine terraces at the margin of some playa-lakes in the Bujaraloz-Sástago area (Gutiérrez-Elorza et al., 2002). This finding opens new prospects to paleoenvironmental investigations in playa-lakes, since terrace deposits, in combination with cores from the lake bottoms, may help to improve the completeness and resolution of lacustrine records. Moreover, lacustrine terraces may be used to reconstruct the morpho-stratigraphic evolution of the playa-lakes and identify major aggradation and excavation periods as potential responses to significant paleoenvironmental changes. Advantages of the terrace deposits, situated at the lake margins and above the water table, with respect to the sediments situated beneath the lake bottoms, include: (1) Higher preservation potential of the stratigraphic record than

98 in the lake bottom, where eolian deflation may remove a substantial amount of
99 sediment. (2) Less severe overprinting by diagenetic processes. (3) They may be studied
100 in natural exposures or excavated trenches, allowing the architecture of the deposits to
101 be analysed and increasing the likelihood of finding datable material. Moreover, the
102 identification of the boundary between lake deposits and weathered bedrock can be
103 carried out with a greater level of confidence in exposures; argillaceous karstic residues
104 are frequently misinterpreted as lacustrine deposits. Once the sequence of lake terraces
105 has been established, the main challenge is to determine the stratigraphic and
106 chronological relationships between the terraces and the deposits situated in the lake
107 bottom. Some of the stratigraphic units identified in cores from the bottom of lakes may
108 not have chronostratigraphic equivalents in terraces and vice versa. The main constraint
109 for integrating such data is the availability of reliable numerical dates.
110
111 This paper is focused on the Bujaraloz-Sastago endorheic area, and particularly on the
112 largest La Playa-El Pueyo lake system. The main goals of this multidisciplinary work
113 include: (1) Evaluating the different hypotheses proposed to explain the origin of the
114 closed depressions developed in evaporitic bedrock in the light of new data on the
115 subsurface geometry of the basin inferred by complementary shallow geophysical
116 techniques (electrical resistivity tomography and seismic refraction). (2) Reconstructing
117 the morpho-stratigraphic evolution of the playa-lake on the basis of the spatial
118 distribution of lacustrine terraces and the obtained numerical dates. (3) Calculating rates
119 of vertical accretion and eolian deflation using the numerical ages obtained for the most
120 extensive terrace. (4) Making an attempt to integrate the terrace (trenches) and lake
121 bottom (cores) stratigraphic records and relate the paleohydrological changes recorded

by the terraces with other paleoenvironmental proxies in the Ebro Depression, the Iberian Peninsula and the global context.

2. The study area

2.1. Geological setting

The study area is located in the central sector of the Ebro Tertiary Basin, NE Spain (Fig. 1). This sedimentary basin, deeply dissected by the fluvial network, constitutes a topographic depression drained longitudinally by the NW-SE-oriented Ebro River and bounded by the Pyrenees and the Iberian Chain to the north and south, respectively**.** The investigated La Playa-El Pueyo playa-lake complex form part of a field of closed depressions with a marked WNW-ESE elongation designated as the Bujaraloz-Sástago endorheic area (Figs. 1 and 2). This internally drained area has been developed on an exhumed structural platform lying at 310-370 m a.s.l., hanging 200 m above the deeply entrenched Ebro River to the south (Fig. 1).

The sedimentary fill in this sector of the Ebro Basin is made up of Oligo-Miocene sediments deposited in evaporite and carbonate shallow lakes and in distal alluvial fan environments (Fig. 1). The strata, showing a very low (<2°) NW to NE dip, form part of the southern limb of a very open WNW-ESE syncline whose pericline is located SE of Bujaraloz (Quirantes, 1978; Arlegui, 1996). The structural platform is underlain by the Lower Miocene Bujaraloz-Sariñena Unit, mostly composed of gypsum, mudstone and limestone (Ramírez, 1997; Solá and Costa, 1997). Salvany et al. (1994, 1996) differentiate two main gypsum-rich units, each underlain by a detrital unit primarily composed of red clays (Fig. 1). From base to top: Middle Detrital Unit (15-20 m),

147 Middle Gypsum Unit (40 m), Upper Detrital Unit (5-6 m), Upper Gypsum Unit (100
148 m). Most of the closed depressions have developed on the Middle Gypsum Unit,
149 exposed in the southern sector of the platform (Fig. 1). This unit has a much lower
150 proportion of clay than the thicker Upper Gypsum Unit. Moreover, the size and spatial
151 frequency of the depressions decrease towards the east, consistently with the wedging
152 out of the Middle Gypsum Unit and the lateral change to marl and carbonate facies
153 (Salvany et al., 1994, 1996). La Playa and El Pueyo playa-lakes occur on the Middle
154 Gypsum Unit, whereas La Salineta has been developed on the Upper Gypsum Unit (Fig.
155 1). The Miocene bedrock is affected by small-throw normal faults with dominant NW-
156 SE azimuths and subvertical joints. Arlegui (1996, p. 217) and Solá and Costa (1997)
157 report a primary N-S trending joint set and a secondary one with E-W orientation.
158 Gutiérrez-Elorza et al. (2002) identified NE-SW and NNW-SSE prevailing joint
159 directions based on 319 measurements taken in limestone beds exposed in La Playa
160 area.
161
162 *2.2. Climate and vegetation*
163 The Ebro Depression has a continental climate, characterized by very hot summers and
164 cold and dry winters. According to the records of Bujaraloz-Petris meteorological
165 station, located 8 km north of the studied playa-lakes, the average annual precipitation
166 and temperature are 360 mm and 14.4°C, respectively. Precipitation shows a bi-modal
167 seasonal pattern, with the highest rainfall in spring and autumn (Rodó et al., 1997).
168 García-Vera (1996) has estimated annual potential evapotranspiration values of 788 and
169 909 mm applying the Thornthwaite and Blaney-Criddle methods, respectively. The area
170 is characterised by a strong wind with prevailing WNW direction locally designated as
171 *Cierzo*. This cold and dry wind blows mainly in winter and spring, channelled along the

172 Ebro Depression and controlled by the presence of anticyclonic conditions in the
173 Cantabrian Sea and low pressures in the Mediterranean Sea (Ascaso and Cuadrat, 1981;
174 Puicercús et al., 1997). At Zaragoza meteorological station, located 60 km to the NW,
175 the maximum wind speed recorded over the period 1942-2010 reached 37.5 m/s (135
176 km/h) in February 1954 with a WNW direction. The data recorded in Bujaraloz
177 anemometric station at 10 m above the ground between March 1991 and January 1993
178 indicate that the highest mean velocities (6-6.5 m/s) correspond to WNW and NW
179 winds, which are the most frequent ones and represent about 75% of the eolian energy.
180 During this period a maximum WNW wind speed of 27.7 m/s (100 km/h) was measured
181 and the wind velocity exceeded 4 m/s around 45% of the time (Puicercús et al., 1997).
182
183 Vegetation landscape in the central Ebro Basin is currently an herbaceous-shrubby land,
184 mostly dedicated to winter cereal farming. Broad leaf tree formations are restricted to
185 humid canyons in elevated areas (Molero et al., 1986; Longares, 1997). Playa-lake
186 basins typically host vegetation dominated by halophytic plant communities, whose
187 distribution reflect water availability and a salinity tolerance gradient (Aguilella and
188 Riera, 1997).
189
190 *2.2. Hydrogeology*
191 The Upper and Middle Gypsum Units constitute two aquifers separated by the Upper
192 Detrital Unit, which behaves as a leaky aquitard (Fig. 1). These gypsiferous
193 hydrostratigraphic units have a rather low average permeability of around 0.01 m/day,
194 largely controlled by solutionally-enlarged joints. Hydraulic permeability reaches the
195 highest values in the bottom of the depressions, due to enhanced karstification by
196 groundwater flow discharge (García Vera, 1996; Salvany et al., 1996; Samper-Calvete

197 and García-Vera, 1998). The groundwater flow in this endorheic area is controlled by
198 the topography of the platform; an extensive plateau riddled by enclosed depressions.
199 Water recharge in the aquifers, estimated at 20-45 mm/yr, flows towards and discharge
200 at the bottom of the main basins, forming local and centripetal groundwater flow cells
201 (García-Vera, 1996; Salvany et al., 1996; Samper-Calvete and García-Vera, 1998;
202 Sánchez et al., 1998). The groundwater salinity increases progressively along the flow
203 path, changing from a Ca-SO_4 composition in the recharge areas, into a Na-(Mg)-Cl-
204 SO_4 hydrochemical facies in the discharge zones (García Vera, 1996; Salvany et al.,
205 1996). Brines in the playa-lakes leads to precipitation of salts at the surface and in the
206 subsurface (Pueyo, 1978/79, 1980; Pueyo and Inglés, 1987). Upward flow and capillary
207 raise in the bottom of the playa-lakes, whose extremely flat topography is controlled by
208 the water table zone, is prompted by the high evaporation rate. The ongoing irrigation
209 plan (Monegros II), affecting 200 km^2 of the endorheic area, will have a significant
210 impact on the hydrology and hydrochemistry (water level raise, dilution, pollution) of
211 these highly sensitive systems with unique habitats and endemic species (García-Vera,
212 1996).
213
214
215 **3. Geomorphology of the playa-lake basins**
216 A total of 99 closed depressions were inventoried by Balsa et al. (1991) in the
217 Bujaraloz-Sátago endorheic area, which covers approximately 250 km^2. According to
218 these authors, the bottom of these topographic basins has a total area of around 8.8 km^2.
219 The majority of the depressions are markedly elongated and oriented in the WNW-ESE
220 direction, which is also the prevailing wind trend. La Playa is the largest lake with 3.5
221 km in axial length and covering 1.72 km^2, approximately 20% of the cumulative area of

the bottom of the depressions (Fig. 2). The structural platform is also carved by poorly hierarchised flat-bottom infilled valleys with dominant WNW-ESE orientation, most of which flow into closed depressions. A significant proportion of the depressions show scarped edges, generally controlled by a laterally extensive limestone bed situated at the top of the Middle Gypsum Unit (Quirantes, 1965). Approximately 20 depressions host ephemeral saline wetlands that get flooded every year (Balsa et al., 1991). These playa-lakes have flat and moist bottoms, indicative of a topography controlled by the water table and the capillary fringe (Rosen, 1994). The largest playas (ie. La Playa, La Salineta) show a slightly more elevated bottom in the southeastern sector, suggesting higher aggradation in the downwind sector by eolian supply and wave action and/or greater erosion in the opposite sector. Water depth reaches the highest values in winter and rarely exceeds 50 cm (Castañeda, 2002; Castañeda et al., 2005). Field and satellite data obtained from 1985 to 2000 indicate that La Playa is one of the playa-lakes with a longer wet cycle, remaining partially flooded more than six months per year (Castañeda, 2002). These elongated lakes tend to have asymmetric geometry in plan view, with higher width in the downwind half than in the windward one, which may have a pointed margin. The leeward margin of La Playa shows an embayment that seems to represent the southeastward expansion of the lake by eolian erosion of the lacustrine terrace situated between this lake and El Pueyo (Fig. 2). Goudie and Wells (1995) indicate that deflation basins excavated in lake deposits within paleolacustrine basins typically display two types of morphologies: (1) Ovoid, almost subcircular, with the long axis perpendicular to the formative air flow. (2) Cusp-shaped, with the apex pointing upwind and oriented parallel to the formative wind. A significant proportion of the playas in the studied area show similar characteristics to the latter morphological type.

247 Progressive evaporation of the brines in the playas leads to precipitation of salts (Pueyo,
248 1978-79; López et al., 1999). Algal mats 3-4 mm thick develop in the playa-lake floor
249 during flooding periods. Saline efflorescences (bloedite, halite and thenardite)
250 precipitate on the lake bottom when the water level recedes. Beneath the surface there is
251 a black sapropelic mud with a high content in sulphides resulting from the reduction of
252 sulphates by bacterial activity. Desiccation cracks develop during dry periods and
253 evolve into saline polygons, eventually framed by teepee-like features as well as bent
254 and overthrusted edges (Fig. 3A). Saline crusts and algal mats locally show blisters
255 formed by the expelling of gases derived from decomposition of organic matter under
256 anoxic conditions and by volume increase related to salt crystallization (Pueyo, 1978-
257 79; Fig. 3B). A very small scarp-edged pit, approximately 30 cm across and 10 cm deep,
258 was identified in the bottom of La Playa lake (Fig. 3C). This feature, very rare in the
259 area, may correspond to a cover collapse sinkhole related to the presence of a cavity of
260 limited size in the gypsiferous bedrock.
261
262 The margins of the lakes typically have an aureole of halofilous vegetation, and wind-
263 trasported particles accumulate in the leeward side of these plants forming elongated
264 nebkha dunes (Fig. 3D). These dunes are frequently made up of sand-sized lenticular
265 gypsum crystals. According to Pueyo (1978-79), these intraclasts result from eolian
266 redeposition of crystals formed in flooded areas and subsequently dried up. Trains of
267 nebkhas may merge resulting in linear dunes several tens of meters long (Fig. 3E).
268 Several processes favour wind deflation in the bottom of the playa-lakes during
269 desiccation periods: (1) Drying cycles involve a significant reduction in cohesion of fine
270 particles, increasing their susceptibility to wind entrainment. (2) Precipitation of salts at
271 the surface may involve the accumulation of light and loose crystals and the preparation

of particles susceptible to deflation by disintegration and salt weathering (i.e. edge of desiccation polygons and collapsed crust blisters; Fig. 3A, B). (3) Trampling by animals (Thomas, 1988; Goudie and Wells, 1995); (4) Accumulation of fecal pellets by worms. Field evidence reveals that this type of biological burrowing activity may predispose a substantial amount of material to wind erosion from the subsurface (Fig. 3F).

Detailed geomorphological mapping was carried out by Gutiérrez-Elorza et al. (2002) in a sector of the endorheic area using a 1:5,000 scale topographic map with a contour interval of 1 m. Three lacustrine terrace levels were identified in La Playa and El Pueyo lakes (Fig. 2). This stepped sequence of terraces records alternating periods during which the lakes were dominated by aggradation or deepening. In La Playa-El Pueyo basin, the upper terrace is represented by a few small benches situated 9 m above the playa-lake bottom in the southeastern margin of El Pueyo lake. The middle terrace, around 6 m above the lake bottom, forms extensive benches in the southeast leeward margin of the playas. The surface of this terrace locally merges with the top of the deposits filling flat-bottomed valleys that drain into the playa-lakes (Fig. 2). The spatial distribution of this terrace reveals that during its accumulation there was a larger single lake around 2.7 km^2 in the depression where La Playa and El Pueyo are located. Subsequently, differential eolian erosion compartmentalized the lake basin into La Playa and El Pueyo, nowadays separated by a remnant of the middle terrace. The lower terrace, with a limited extent, is situated at about 0.5 m above the lake bottom. This apparently very recent level forms discontinuous benches at the margins of the playa-lakes, mainly in the windward sector. It is not clear whether the current lake bottom is a strath surface cut-across the deposit of the lowest terrace or the aggradation surface of an inset younger stratigraphic unit.

The modern La Salineta Lake, 0.2 km^2 in area, lies within a much larger paleolake, whose deposits have been partially eroded and form scarps up to 4 m high surrounding the present lake. Two main terraces have been recognized. The upper terrace is best developed at the southeastern end of the basin. Remains of another small terrace at a relative height of 1 m occur at several locations.

A total of 50 yardangs up to 264 m long with a dominant WNW-ESE trend have been mapped in the leeward side on the largest playas, mainly La Playa (1.72 km^2), El Pueyo (0.14 km^2) and El Pito (0.35 km^2) lakes (Gutiérrez-Elorza et al., 2002; Figs. 2 and 4). Yardangs are elongated hills produced by wind erosion in combination with other process such as weathering and gullying. To our knowledge, these are the only yardangs reported in Europe (Goudie, 2007). The spatial distribution of the yardangs is attributed to the higher abrasive capability of the wind in the leeward sector of the larger playas, due to enhanced concentration of particles in the air currents by deflation. Most of these landforms have been developed in gypsiferous bedrock, and a few of them have been carved on unconsolidated terrace deposits (Fig. 4). These landforms provide evidence of the geomorphic effectiveness of wind erosion in the area. Additionally, the yardangs formed in the middle lake terrace deposits strongly suggest that wind erosion has played a significant role in the geomorphic evolution of the playa-yardang systems in recent times.

Several hypotheses have been proposed to explain the origin of the closed depressions in the Bujaraloz-Sástago endorheic area. According to one interpretation, the basins result from differential dissolutional lowering of the ground surface controlled by

322 fractures (Mingarro et al., 1981). These would be solution sinkholes generated by
323 downward vadose flows in the epikarst zone (Williams, 2004; Beck, 2005; Gutiérrez et
324 al., 2008a; Gutiérrez and Cooper, 2011). This model is not compatible with the
325 available hydrogeological data, indicating that the playa-lake basins essentially behave
326 as discharge zones. Several researchers explain the depressions as the result of the
327 brittle collapse of cavities generated by structurally controlled subsurface dissolution of
328 the gypsum bedrock (Aramburu, 1904; Quirantes, 1965; IRYDA, 1989). This
329 explanation, which involves the development of cavities beneath the platform, fits with
330 the bedrock collapse sinkholes of several genetic classifications (Williams, 2004; Beck,
331 2005; Gutiérrez et al., 2008a). However, no significant karstic voids have been found in
332 the boreholes drilled in the area (M.A. García-Vera pers. comm.). The sole small
333 collapse feature identified in La Playa is most likely related to the presence of rare
334 karstic conduits of limited size (Fig. 3C). Another hypothesis involves a mixed karstic
335 and eolian origin (Sánchez et al., 1998; Desir et al., 2011). Initially, the depressions may
336 form and evolve as solution sinkholes by percolating water in the vadose zone.
337 Infiltration is favoured by the horizontal topography of the platform (Ibáñez, 1975).
338 Once the bottom of the dolines reaches the water table zone, local groundwater flow
339 cells that discharge in the depressions are established. The underground flows that
340 converge in the basins cause widespread dissolution of the bedrock, leading to gradual
341 subsidence. During certain periods, the strong WNW prevailing winds may cause the
342 erosional lowering of the floor of the basins by deflation. According to this
343 interpretation, the genesis of the depressions involves processes characteristic of
344 solution sinkholes, deflation basins and subsidence sinkholes (Williams, 2004;
345 Gutiérrez et al., 2008; Goudie and Wells, 1995). From the hydrogeological point of

346 view, this evolutionary model implies the transformation of a recharge basin into a
347 hydrologically closed discharge playa (Rosen, 1994; Yechieli and Wood, 2002).
348
349 The origin and hydrogeology of the depressions is particularly important from the
350 stratigraphic and paleoenvironmental record perspective (Rosen, 1994). The
351 preservation potential of the lake sediments in the bottom of the depressions would be
352 higher if bedrock collapse is the main genetic process. This subsidence mechanism
353 would lead to a lacustrine fill with highly variable thickness and affected by
354 gravitational deformation. Several geophysical surveys have been acquired in La Playa
355 depression aimed at characterizing the geometry of the lake deposit and testing the
356 different genetic hypotheses.
357
358
359 **4. The previously studied lacustrine sequences**
360 A number of sequences from playa-lakes in the Bujaraloz-Sástago area have been
361 investigated (Pérez-Obiol and Roure, 1990; Stevenson et al., 1991; Davis, 1994; Schütt,
362 1998; Davis et al., 2003; Moreno et al., 2004; Valero-Garcés et al., 2004; González-
363 Sampériz et al., 2008; Mees et al., 2011). The last review by González-Sampériz et al.
364 (2008) summarized the vegetation changes and moisture fluctuations since the Last
365 Glacial for the central sector of the Ebro Depression and included a detailed description
366 of two cores retrieved from La Playa and La Salineta playa-lakes. Available
367 chronologies only allow a millennial scale reconstruction. According to this review, the
368 early Holocene was the wettest period, and the common lack of most Holocene
369 sediments in the lake basins would have been caused by an intensification of eolian
370 deflation under arid conditions during the Mid Holocene. Moreover, the records indicate

371 relatively more humid conditions during the late Holocene after 4 ka, with more
372 frequent flooded conditions in the lake basins.
373
374 *4.1. La Salineta*
375 An outcrop of a lacustrine terrace located in the southeastern margin of La Salineta (0-
376 360 cm) and a core (360-465 cm) collected in the lake bottom, at the foot of the terrace
377 riser, were described and sampled by Davis (1994). Chenopodiaceae seeds from the
378 upper 20 cm of the 465 cm long La Salineta section gave a modern AMS age probably
379 caused by soil contamination, and consequently the chronology of this section is
380 unknown.
381
382 An 8 m long core (La Salineta Core) was drilled in the upper terrace close to the
383 previous section, providing one of the longest lacustrine records available in the central
384 Ebro Depression (Fig. 5). The core reached the bedrock composed of Miocene
385 limestone (Valero-Garcés et al., 2004). No terrestrial macro organic remains were found
386 in the core, so the chronology is constrained by bulk organic matter AMS radiocarbon
387 ages. The section reaches the Late Glacial Maximum (LGM, around 20 ka cal. BP) and
388 contains the Late Glacial and early Holocene, although the chronology of the upper half
389 of the sequence is not constrained. AMS samples from the upper 3 m gave modern ages,
390 although pollen indicators suggest that the sequence contains recent Holocene (last
391 millennium) sediments.
392
393 The modern Salineta playa-lake bed lies about 4 m below this terrace. An 87 cm long
394 sediment core was recovered by González-Sampériz et al. (2008) in the center of the
395 lake. These authors described three depositional sequences (S-III, S-II and S-I) bounded

by erosional hiati. Chronological control is restricted to a radiocarbon age from a pollen concentrate obtained in sequence S-II at 65-67 cm below the surface (2131-1966 cal yr BP). The presence of dolomite, the more positive $\delta^{18}O$ values pointing to intense evaporative processes, the maximum values of clays and quartz and the dominance of halophytic terrestrial plants, as suggested by $\delta^{13}C_{org}$ values (-26‰), indicate relatively carbonate-dominated brine and an ephemeral lake system with frequent desiccation periods during deposition of undated S-III (prior to 2000 cal yr BP). Sequence S-II would represent deposition in an ephemeral playa-lake dominated by gypsum-rich sediment formation pointing to a different brine composition after 2000 cal yr BP. Finally, sequence S-I represents deposition during the present-day ephemeral saline lake, characterized by higher content of the more soluble sulphates and the dark-grey, banded to black laminated nature of the sediments. Although the chronological control is poor, sedimentological and palynological data (i.e., arboreal component less than 40% and continuous presence of *Cerealia*) indicate that these sediments are of recent Holocene age.

4.2. La Playa

In the 162 cm long core from the western margin of La Playa, González-Sampériz et al. (2008) differentiated three depositional sequences (P-III, P-II and P-I) bounded by erosional surfaces (Fig. 5). This succession and the pollen record, particularly the ratio between halophytes (Chenopodiaceae) and steppe taxa (*Artemisia*) *versus* aquatic plants (*Ruppia, Myriophyllum, Potamogeton*), record a depositional history characterized by the evolution from a carbonate-producing lake (Units P5, P4 and P3) towards a more sulphate-producing saline lake (Unit P2) some time before 9.7 ka, ending with the present-day ephemeral saline lake system (Unit P1). The upper Unit P1 is characterized

421 by deposition of calcitic, organic-rich mud with abundant gypsum microcrystals and
422 without the halite crust characteristic of other playa-lakes in the area. The main
423 limitation of this record is the poor chronological control; only one age is available from
424 the middle part of depositional sequence PII (80 cm below the surface, 9914-9676 cal yr
425 BP; Fig. 5). The chronology of the depositional sequences and the erosional hiati at the
426 boundary between them is unknown. The available data suggest that early Holocene
427 deposits were preserved at the base of the sequence, but most of the Holocene sediments
428 have been eroded and the age interval of the middle sequence is unknown. The top
429 sediments (Unit P1) represent historic and recent deposition taking into account the
430 pollen content (*Olea* and Cerealia cultives). The mineralogical study by Mees et al.
431 (2011) based on profile pits and auger holes from 14 basins in this endorheic area shows
432 a similar recent stratigraphy.
433
434 **5. Methods**
435 Three trenches have been excavated to investigate the deposits of the upper and middle
436 terraces of La Playa-El Pueyo lake system at two sites (Figs. 2, 4, 7 and 8). The
437 trenching technique is mainly applied to assess the seismogenic potential of active faults
438 in paleoseismological studies (McCalpin, 2009, 2011). However, its practicality has
439 also been proved in the study of sinkholes (Gutiérrez et al., 2009), landslides (Gutiérrez
440 et al., 2008b, 2010) and various types of surficial deposits; fluvial (Brackenridge, 1985),
441 eolian (Mahan et al., 1999), etc. In this study, after cleaning the vertical trench walls, a
442 reference grid with horizontal and vertical strings spaced 0.5 or 1 m apart was placed on
443 one of the flanks of each trench (Fig. 7B). The stratigraphy of the selected walls was
444 logged on graph paper with the aid of the grid and a tape measure (Fig. 8). Colour pins
445 were nailed at stratigraphic contacts to facilitate the mapping and sampling process.

Sedimentary facies were described in the trench according to sedimentary textures and structures, grain size and sediment composition. Twenty six samples were collected in the 5 m thick sequence of the middle terrace exposed in one of the trenches for clay fraction and elemental composition (Total Organic Carbon, Total Inorganic Carbon, Total Sulfur). Grain size analyses were performed with a Coulter Grain Analyzer after removing organic matter with oxygen peroxide and a treatment with ultrasounds and clay dispersants. TOC, TIC and TS analyses were performed with a LECO elemental analyzer. Pollen samples were taken in the upper (2 samples) and middle (18 samples) terrace of La Playa-El Pueyo lake system. The chemical treatment of these samples has followed the usual method that includes HF, HCl, KOH and Thoulet density 2.0 heavy liquid (Dupre, 1992). However, the pollen preservation was very low, and most samples were sterile or with very poor taxonomic diversity. Thus, a vegetation or chronological comparison between the lacustrine core (González-Sampériz et al., 2008) and the trench sequences was not possible.

Seismic refraction and electrical resistivity tomography (ERT) profiles were acquired in La Playa lake. Seismic refraction utilizes seismic compression waves refracted at the interface between units with different propagation velocities and recorded by a seismograph and a linear array of geophones at the surface. The analysis of the first-arrival times of direct and critically refracted waves allows modelling the depth profile of refractor contacts and the propagation velocity (v_p) of each layer. Seismic refraction was selected as an adequate method to investigate the depth and geometry of the boundary between the nonconsolidated lake deposits and the gypsiferous bedrock (i.e. Hetch, 2003; Hoffman and Schrott, 2003; Schrott and Sass, 2008). Lines of P-wave

471 refraction data were acquired using a 12-channel Geometrics Strataview seismograph,
472 10 Hz geophones and a sledgehammer energy source. Spacing in the geophone arrays
473 was 5 m, except for the first and last geophones located at 2.5 m from the first and last
474 shot points, respectively. Three shot points were used with each spread, enough to
475 obtain information on the geometry and properties of shallow layers. The span of the
476 traverses was constraint to 55 m both by the available cable length and the ability to
477 generate sufficient energy with the sledgehammer through unconsolidated lake deposits.
478 The recorded seismic data was processed using the SIPT2 iterative inversion refraction
479 analysis software, which generates the first solution by a delay-time method, while
480 subsequent iterations modify the solution through ray tracing (Scott, 1973).
481
482 Electrical resistivity tomography (ERT) allows imaging spatial variations in the
483 electrical resistivity of subsurface materials by processing electrical measurements from
484 electrode arrays (i.e. Griffiths and Barker, 1993; Sumanovac, 2006). Bulk electrical
485 resistivity (ρ), the resistance of the ground to the passage of an electric current, is
486 determined by the amount of conducting minerals and specially the chemical
487 composition of interstitial water. It may be used to identify the boundary between
488 different units, like the bedrock-cover interface (Samouëlian et al., 2005; Schrott and
489 Sass, 2008; Van Dam, 2010). It may also image resistivity variations related to changes
490 in the amount and chemistry of impregnating waters within the same geological unit
491 (i.e. Bauer et al., 2006; Cassiani et al., 2006; Leroux and Dahlin, 2006; Poulsen et al.,
492 2010).). For example, the electrical resistivity of meteoric water derived from
493 precipitation ranges between 30 and 1000 Ωm, whereas that of sea water is generally
494 about 0.2 Ωm (Bell, 2007). ERT was *a priori* an adequate method to delineate the
495 rockhead and to infer electrical changes related to permeability and hydrochemical

496 variations. To our knowledge, there are no publications dealing with the application of
497 this method in playa-lakes. The ERT profiles were acquired with a multi-electrode Lund
498 Imaging System (ABEM). The system is composed of a Terrameter SAS 1000,
499 electrode selector ES10-64 and 4 signal cable and reels and 64 steel electrodes. We
500 selected a Wenner electrode array. Although this configuration provides lower
501 horizontal resolution than the dipole-dipole array, it has a greater signal-to-noise ratio,
502 yields tomographs with good vertical accuracy and may also provide a reasonable
503 horizontal resolution, especially if the spacing between electrodes is reduced (i.e.
504 Sasaki, 1992). The interelectrodic spacing (a) used was alternatively 1 or 2 m for the 40
505 central electrodes and 2a for the 24 electrodes on both ends of the line. This ensured
506 enough resolution, especially in the central sector of the profile, without compromising
507 the required investigation depth. The measured apparent resistivity (ρ_a) data were
508 processed using the 2D finite-difference inversion commercial software RES2DINV of
509 Loke and Barker (1996). The program employs a 2D model of rectangular cells,
510 producing through inversion of the raw data a true resistivity value for each node and an
511 electrical resistivity tomograph.
512
513 **6. Results**
514 *6.1. Geophysical investigation*
515 The seismic refraction and ERT profiles have been acquired along an E-W trending
516 trace across La Playa, including the middle terrace at the NE margin (Fig. 6A). In order
517 to use subsurface direct data for the interpretation of the profiles, the selected trace met
518 the location of a borehole drilled in the lake bottom (González-Sampériz et al., 2008)
519 and the trenches excavated in the middle terrace (Fig. 6A, B). A total of 4 ERT profiles
520 (T1a, T1b, T2 and T3) and 2 seismic refraction traverses (SR1, SR3) have been

521 acquired in three sections of the selected trace. ERT profiles T1a (80 m) and T1b (160
522 m), centred at the scarp of the middle terrace next to the trenches, investigate both the
523 terrace and the lake bottom margin. Profile T1b was acquired with an electrode spacing
524 of 2 m, whereas the spacing in profile T1a was 1 m in order to get higher resolution.
525 The location of the 55 m long traverse SR1, performed on the terrace surface,
526 essentially coincides with the eastern half of the electrical resistivity profiles T1a and
527 T1b. ERT profiles T2 and T3, both 80 m long and with an electrode spacing of 1 m,
528 were carried out in the central and western sector of the lake bottom, respectively. The
529 core investigated by González-Sampériz et al. (2008) was obtained between profiles T2
530 and T3. The 55 m long SR2 seismic traverse roughly coincides with the eastern half of
531 the ERT profile T3.
532
533 The seismic refraction profile SR1 carried out in the middle terrace reveals two main
534 seismic units with markedly different velocities (see dashed lines in Fig 6C). The upper
535 unit, with homogeneous behaviour and attributable to the terrace deposit and probably
536 also to the underlying clay-rich karstic residue, has an average velocity of 400 m/s. At
537 the top of this unit there is a thin layer with a lower average velocity of 291 m/s that
538 corresponds to the uppermost deposits of the terrace disturbed by ploughing. The higher
539 thickness and channel-like base of this subunit in the eastern sector coincides with a
540 very gentle erosional trough, suggesting the presence of higher porosity alluvial
541 deposits and/or man-made ground. The lower unit, which corresponds to the bedrock,
542 has a dip-corrected velocity of 3664 m/s. According to the seismic refraction profile
543 SR1, the rockhead has an overall planar geometry and is situated at ca. 5 m in depth in
544 the vicinity of the terrace scarp, coinciding with the position of the top of the fresh
545 bedrock exposed in the trench dug at the terrace scarp. The ERT profiles T1a and T1b

546 show a sharp resistivity change at approximately the same depth beneath the terrace.
547 This geophysical contact shows a slight dip towards lake and profile T1a displays an
548 apparent west-facing step at the reference point 8 that may be related to local changes in
549 the karstic residue. The resistivity of the terrace deposits varies significantly with the
550 distance to the surface, both the terrace tread and scarp. The material situated close to
551 the ground has resistivity values of 6-25 Ωm and decreases away from the surface to 1-6
552 Ωm. This resistivity distribution pattern may be explained by differences in soil
553 moisture betwwen the surface material and the subsoil. The sections of the ERT profiles
554 T1a and T1b situated at the lake bottom next to the terrace scarp do not allow inferring
555 with confidence the position and geometry of the cover-bedrock contact. The complex
556 resistivity pattern recorded in this sector may be related to different factors, including:
557 (1) Significant lateral changes from lacustrine to colluvial facies associated to the 6 m
558 high terrace riser. The deposits at the foot of the scarp may incorporate fallen blocks of
559 terrace deposit as suggests the high resistivity anomaly shown between the reference
560 lines 20 and 14 in profile T1a. (2) Variations in electrical resistivity related to changes
561 in water content and salinity, controlled by changes in porosity and the position of the
562 water table and capillary fringe. (3) The probable presence of a fresh water - brine water
563 interface at the lake margin dipping away from the basin (Samper et al., 1993; García-
564 Vera, 1996; Yechieli and Wood, 2002).
565
566 The main findings of the seismic refraction traverse (SR2) and the ERT profiles (T2 and
567 T3) carried out in the bottom of the lake include (Fig. 6C): (1) The unconsolidated lake
568 deposits plus the underlying karstic residue have average v_p = 301 m/s and ρ < 1 Ωm.
569 This unit has an overall planar base situated at 1-2 m below the surface, in agreement
570 with the position of the top of the bedrock identified in three boreholes drilled in this

571 lake. González-Sampériz et al. (2008) found the top of the bedrock at 1.62 m in a core
572 located between profiles T2 and T3. Pérez-Obiol and Roure (1990) and Stevenson et al.
573 (1991) reached the rockhead in boreholes perforated in La Playa bottom at 1.1 and 2.3
574 m below the surface, respectively. The low-relief irregularities that display the base of
575 this low electrical resistivity unit may be related to lateral changes in thickness and
576 composition of the karstic residue. That is, a slightly irregular rockhead typical of
577 mantled karst settings. (2) The seismic refraction traverse SR2 reveals two seismic units
578 within the bedrock at approximately 6 m beneath the surface, that may correspond to
579 two zones with different degree of karstification or to two lithological units of the
580 horizontally lying Miocene sequence. The upper one has an average v_p = 1549 m/s and
581 the lower one v_p = 4290 m/s. Bulk resistivity in the bedrock range from ρ = 2 to 12 Ωm.
582 The higher electrical conductivity of the bedrock beneath the lake than at the margin of
583 the depression may account for the presence of higher salinity phreatic water in the
584 former. Profile T2 performed in the central sector of the lake, shows vertical fringes
585 with lower resistivity attributable to zones of preferent brine discharge related to
586 fracture and dissolution enhanced permeability.
587
588 *6.2. Lake terraces. Stratigraphy*
589 The middle terrace was investigated by means of two adjacent trenches dug in the NE
590 margin of La Playa (E735927 N4589264; Figs. 2, 4, 7, 8). Initially, we dug a trench by
591 hand in the terrace scarp, extending from the top of the terrace to the base of the karstic
592 residue situated between the lacustrine deposit and the bedrock (Figs. 7A and 8). This
593 N70E trending trench with stepped base was 10 m long, 1 m deep and 0.6 m wide. It
594 provided an exposure with limited lateral extension (0.5-2 m) of the 5 m thick terrace
595 deposit. Subsequently, a backhoe trench with N160E orientation was excavated next

596 and parallel to the terrace scarp (Figs. 7B, C, 8). The aim of this trench was to obtain a
597 wider picture of the upper deposits of the terrace, in order to better characterise their
598 geometry and architecture and to increase the likelihood of finding datable material. The
599 depth of this 11 m long trench was limited to 3.1 m due to safety reasons. This backhoe
600 trench was connected to the hand-dug trench by a subsidiary trench in order to establish
601 a physical correlation between the upper stratigraphic units identified on both trenches
602 (Figs. 7C and 8). A synthetic stratigraphic log has been produced for the terrace; the
603 lower 188 cm were described in the hand-dug trench and the upper 312 cm in the higher
604 quality exposure of the backhoe trench (Fig. 9).
605
606 Three main units have been identified in the trenches (Fig. 8): (1) Bedrock
607 composed of slightly weathered and horizontally lying alabastrine nodular gypsum with
608 marl intercalations. (2) A karstic residue 45 cm thick made up of highly cohesive dark
609 grey marl with residual gypsum particles up to 1 cm long. The top of both the bedrock
610 and the karstic residue are slightly inclined towards the lake, as it was interpreted from
611 the ERT profiles (Fig. 6). (3) A l5 m thick lake terrace deposit, in which 25 layers have
612 been differentiated. The uppermost unit, 39 cm thick, corresponds to lacustrine
613 sediments disturbed by ploughing. The hand-dug trench exposed in the upper part a
614 sediment-filled conduit 50 cm across cross-cutting several layers (Fig. 8). This feature
615 corresponds to a biogenic burrow, probably related to a fox or rabbit den. Pollen content
616 in the 18 samples collected in the trench is very low (less than 30-40 grains) and they
617 contain only pine, some Chenopodiace, Poaceae and isolated grains of *Artemisia* and
618 Fabaceae, preventing any. palynological analysis..
619

620 The terrace deposit is primarily composed of tabular and horizontally-bedded
621 massive or vaguely laminated gypsiferous sands and silts (Fig. 8). A significant
622 proportion of lenticular gypsum crystals occurs in some beds, most likely precipitated in
623 the playa-lake bottom or within the sediments from interstitial water (Pueyo, 1978-79;
624 Pueyo and Inglés, 1987). The gypsum crystals may be in place or may have been
625 reworked as intraclasts by eolian or wave currents. Some beds (4, 7, 17, 21, 22) that
626 may include granule-sized particles show an undulated erosional base recording higher
627 competence water flows at the lake margin (Fig. 9). Layer 17 corresponds to a 50 cm
628 wide and 8 cm deep channel filled with massive dark grey-brown sandy silt with
629 charcoal fragments up to 5 mm long and abundant bioturbation (Fig. 8). The top of layer
630 3 includes centimetre-size silt rip-up clasts probably reworked from mud cracks. Layer
631 18 displays faint undulated lamination attributable to ripples. Several depositional
632 sequences 11-35 cm thick can be recognized in the middle part of the terrace deposit.
633 These sequences typically consist of light-coloured gypsiferous sand or silt with an
634 erosional or planar base and a darker and finer-grained gypsiferous facies with abundant
635 bioturbation at the top. The base of the darker upper part, with higher content in organic
636 matter, may be net or gradational. The bioturbation-related porosity is largely filled by
637 white secondary carbonate. These depositional sequences may record flooding events in
638 the lake, starting with an erosional water flow event, a lake level increase with
639 progressive dilution favoring the proliferation of biota in the lake bottom and the
640 accumulation-preservation of organic matter (higher productivity and/or preservation of
641 organic matter).
642
643 Grain size and compositional analyses also identify four main units above the
644 rockhead, including the basal 45 cm karstic residue, the top 39 cm sediments altered by

645 farming, and two main units within the lake sediments in the terrace (Fig. 9). The lower
646 terrace unit (20 to 26 layers, 210 – 391 cm depth) is characterized by finer clayish silt
647 sediment (up to 50% clay size particles) with the lowest organic (less than 1 %) and
648 carbonate (less than 1 %) content and the highest sulfur content (up to 1.5 %) of the
649 whole sequence. These features suggest a sulfate-rich brine lake more conducive to
650 gypsum deposition. The transition to the upper unit at about 210 cm depth is rather
651 sharp and the upper sediments in the trench are dominated by coarser particles (40 %
652 clay size) with relatively higher organic (up to 1.5%) and carbonate (up to 1.5%)
653 content and lower sulfur content (< 0.5%). The upper 1 m thick unit is slightly coarser.
654 Lower gypsum content, the relatively coarser nature of the sediments and the presence
655 of numerous fining upward sequences are indicative of a less saline environment and
656 the occurrence of frequent flooding episodes in the basin.
657
658 A 4 m long and 1 m deep trench with N40E orientation was dug by hand in a
659 bench ascribed to the upper terrace located southeast of El Pueyo lake (E736799
660 N4588450; Figs. 2 and 4). This terrace remnant, at about 9 m above the lake bottom, is
661 situated at the windward edge of a bedrock yardang and is surrounded by an extensive
662 inset surface of the middle terrace. The trench exposed massive yellowish white
663 gypsiferous silts 75 cm in thickness overlying an erosional base carved in Miocene
664 limestone bedrock. The deposit includes a discontinuous bed of angular cobble-size
665 limestone clasts. This deposit is clearly more indurated (cemented) than those of the
666 younger middle terrace. The geomorphic setting and the sedimentological
667 characteristics suggest deposition at the lake margin affected by both lacustrine
668 sedimentation processes and slope wash responsible for the accumulation of clasts
669 derived from the nearby bedrock outcrop. The limited thickness of the deposit may be

related to its marginal position and postdepositional erosional lowering of the terrace surface.

6.3. Chronology and morpho-sedimentary evolution

Charcoal samples from the middle terrace with enough organic carbon content for AMS ^{14}C dating were collected from layers 1, 11, 14, 17, 21 and 23 at 20, 221, 256, 294, 330, 385 and 405 cm above the base of the deposit, respectively (Figs. 8 and 9; Table 1). These samples yielded the following calibrated ages consistent with their stratigraphic order: 3887-3699, 3512-3383, 3638-3465, 3085-2925, 2742-2461, 2158-1995, 487-311 cal yr BP (2 sigma calibrated age ranges with a relative probability greater than 0.80). The anomalous modern age of the uppermost sample, collected at 95 cm below the terrace surface, is attributed to soil contamination. Relatively large pieces of charcoal were collected from an approximately 50 cm thick bed exposed at the terrace scarp at some distance from the trenches, providing a calibrated age of 3269-3060 cal yr BP. The sampled sediments were visually correlated with the upper part of layer 1. However, the large deviation between the obtained numerical age and the chronological model constructed with the better stratigraphically constrained trench-derived ages suggests that such correlation was erroneous (Fig. 10). Most likely the analysed charcoal corresponds to a younger lacustrine bed or to a colluvial deposit derived from more recent lake deposits.

Unfortunately, we did not find any suitable material for ^{14}C dating in the trench dug in the upper terrace. Two samples (UTL1 and UTL2) were collected for optically stimulated luminescence (OSL) dating from the massive gypsiferous silts situated above and below the layer of limestone clasts, at about 45 and 15 cm above the base of the

695 deposit, respectively (Fig. 11A). Details of the OSL dating procedures and equipment
696 employed in this study are provided in the online Supplementary Information.
697
698 Sample UTL2 did not yield sufficient quartz grains for equivalent dose (D_e) estimation.
699 However, we were able to obtain finite D_e estimates for 133 of the 900 grains analysed
700 from sample UTL1 (Fig. 11B). Sample UTL1 yielded a single-grain OSL age of 128±9
701 ka and an associated multi-grain aliquot OSL age of 127±18 ka (boooth calculated using
702 the 4-parameter minimum age model (MAM-4) of Galbraith et al., 1999; Table 2). The
703 obtained age of the analysed sample is much older than might be expected considering
704 its morphostratigraphic position. The upper terrace is situated just 3 m above the middle
705 terrace, so it is highly improbable that the two deposits are separated by >100 ka and
706 there are no evidences of other Late Pleistocene or Early Holocene high-stand terraces.
707 Moreover, the preservation of unconsolidated lake deposits at the windward edge of a
708 yardang over a 128 ka period seems unlikely. The terrace might correspond to a strath
709 surface developed on much older deposits. Additional discussions about the reliebility
710 of the OSL age are provided in the online Supplementary Information.
711
712 The mapped sequence of terraces reveals that the La Playa-El Pueyo lake basin has been
713 dominated by an overall deepening trend throughout its evolution (Fig. 12). The terraces
714 record interruptions in this trend at times during which the lake was dominated by
715 aggradation. Unfortunately, we only have one OSL numerical age for the upper terrace
716 (ca. 128 ka) whose reliability is difficult to assess independently and the chronology of
717 the lower terrace level is poorly constrained; though it is likely to be recent Holocene in
718 age and probably historical. Regarding the middle terrace, at the trench site, the
719 accumulation of lacustrine deposits 5 m thick occurred from ca. 3.9 ka to soon after 2

720 ka, yielding a maximum average aggradation rate of 2.6 mm/yr. Using the ages of the
721 samples collected in units 1 and 23 we can estimate an average vertical accretion rate of
722 2.1 mm/yr. According to the chronological model (age *vs.* distance to base), aggradation
723 was much more rapid during deposition of the lower half of the sequence; 8.3 mm/yr
724 between layers 1 and 14, and 0.9 mm/yr between layers 14 and 23 (Fig. 10).
725 Considering the approximate area of La Playa-El Pueyo lake during the deposition of
726 the middle terrace (2.73 km^2) and assuming that 5 m of sediments were accumulated on
727 average during this aggradation phase, we can estimate a total sedimentary input of
728 13.65 million m^3. This volume, incorporated in a minimum time span of 1.9 ka, yields a
729 maximum sedimentary input rate of 7184 m^3/yr and a specific value of 26.31 m^3/ha/yr.
730
731 Subsequent to the accumulation of the middle terrace, the lake bottom underwent
732 entrenchment attributable to wind deflation during periods of low water tables. This
733 erosional lowering phase was interrupted by a brief aggradation period in recent times,
734 probably historical, recorded by the lower terrace. Differential erosion resulted in the
735 segmentation of La Playa and El Pueyo lakes (Fig. 12). Considering that the top of the
736 deposits of the middle terrace is situated 5.95 m above the lake bottom and that the
737 erosional phase started sometime after 2 ka, we can estimate a minimum mean vertical
738 erosion rate due to wind deflation of 3 mm/yr. This minimum rate also applies to the
739 yardangs carved in the deposits of the middle terrace. Additionally, considering the
740 current area of La Playa and El Pueyo lakes (1.72+0.14 km2) and the relative height of
741 the terrace (5.95 m), we can estimate that eolian deflation has evacuated a volume of
742 around 11.07 million m^3 in La Playa-El Pueyo lake system in a time period shorter than
743 2 ka. This means a maximum long-term erosion rate of 5,533 m^3/yr and a specific rate
744 of 30 m^3/ha/yr.

745

746 The long-term deflation rates estimated for La Playa-El Pueyo lake system compares
747 well with those calculated in several arid regions of the world, generally using yardangs
748 carved in Holocene lake deposits. McCauley et al. (1997) indicate rates of 20 mm/yr for
749 the Lop Nor yardangs in Central Asia. The data presented by Anderson et al. (2002) on
750 the Laguna del Perro, a deflation basin within the pluvial Estancia Lake in New Mexico,
751 indicate a surface lowering rate of ca. 3 mm/yr. Excavation rates ranging between 0.4
752 and 4 mm/yr have been reported in lakes for post-Neolithic pluvial periods (Cooke et
753 al., 1993 and references therein). Goudie et al. (1999) estimate wind erosion rates
754 between 0.5-1.7 mm/yr over the last 4.5-5 ka at Kharga Oasis, Egypt. In Sebkha
755 Mellala, Algeria, a deflation rate of 0.4 mm/yr has been estimated for the last 6-7 ka
756 (Boyé et al., 1978). In the last 2 ka, differential wind erosion has operated at rates of
757 0.5-2 mm/yr in relict mantled pediments in Algeria. Present-day deflation rates in the
758 Bodélé Depression, Chad, a pluvial lake filled with diatomites which constitutes the
759 planet's largest single source of dust, are of the order of 3 mm/yr (Washington et al.,
760 2006). In Ebinur Lake, NW China, measured contemporaneous deflation rates range
761 from 2.4 to 9.6 mm/yr (Liu et al., 2011).

762

763

764 **7. Discussion and conclusions**

765 Two main interpretations have been proposed to explain the origin of the lake basins in
766 Bujaraloz-Sástago area: (1) Collapse of large karstic cavities developed within the
767 evaporite bedrock. (2) Widespread subsurface dissolution and subsidence in
768 combination with eolian deflation. The overall tabular geometry of the lake fill, with no
769 significant thickness changes inferred from the ERT and seismic profiles acquired in La

770 Playa, strongly support the second alternative. Once the bottom of solution sinkholes
771 reaches the water table, local groundwater flows that discharge in the lakes cause
772 widespread dissolution of the bedrock and gradual settling of the lake sediments. The
773 gypsum removed from the bedrock as solutes precipitates in the lake contributing to
774 vertical accretion. Under favourable conditions, when the lake dries out, the lacustrine
775 sediments are evacuated by wind deflation causing the erosional lowering of the basin
776 floor. This genetic model is also supported by: (1) the limited thickness of the deposits
777 underlying the lake, including significant erosional hiati (Moreno et al., 2004;
778 González-Sampériz et al., 2008), (2) the occurrence of terrace deposits at the margins of
779 the lakes that do not seem to have correlative units in the lake bottom, (3) the presence
780 of yardangs carved in bedrock and terrace deposits in the leeward side of the largest
781 playas, (4) the rapid development of nebkha dunes and (5) the absence of significant
782 cavities in the boreholes drilled in the area.
783
784 The studied lake basins have been dominated by an overall deepening trend during their
785 evolution, episodically interrupted by net aggradation periods recorded by lacustrine
786 terraces (Fig. 12). The upper terrace, situated at 9 m above the lake bottom, records the
787 oldest accumulation phase with preserved geomorphic expression. Most likely the
788 limited thickness of the deposit (75 cm) found in the trench excavated in this terrace is
789 related to the marginal position of the site and to post-depositional erosion. We have
790 obtained a single OSL age of ~128 ka from this level. Further chronological control is
791 needed to assess the validity of this age estimate.
792
793 The middle terrace is situated at 6 m above the lake bottom and at the trenching site the
794 deposit of this morpho-stratigraphic unit is 5 m thick. This indicates that the lake bottom

795 underwent a minimum deepening by deflation of 8 m between the accumulation of the
796 upper and middle terraces. The middle terrace records a net aggradation phase of at least
797 5 m between 3.9 ka and soon after 2 ka. The lowest and upper dated layers allow the
798 estimation of a maximum average vertical accretion rate of 2.6 mm/yr. The
799 chronological model reveals that aggradation occurred at a much higher rate during the
800 lower half of the sequence than in the upper one (8.3 *vs* 0.9 mm/yr). The spatial
801 distribution of the middle terrace indicates that during the accumulation of this unit La
802 Playa and El Pueyo lakes were integrated into a larger single lake.
803
804 The subsequent excavation period was interrupted by a brief aggradation phase recorded
805 by the lower terrace, situated a 0.5 m above the lake bottom. During this major
806 erosional phase, differential eolian deflation excavated the depressions of La Playa and
807 El Pueyo lakes, separated by remnants of the middle terrace. This involved a reduction
808 of the lake area from 2.73 km^2 to 1.86 km^2. Considering that the erosional phase started
809 soon after 2 ka, we can estimate a minimum mean vertical erosion rate due to wind
810 deflation of 3 mm/yr. This minimum rate also applies to the yardangs carved in the
811 deposits of the middle terrace. The apparently high long-term deflation rate estimated
812 for La Playa-El Pueyo lake system compares well with those calculated in several arid
813 regions of the world using yardangs carved in Holocene lake deposits, as we have
814 mentioned above (Washington et al., 2006 and references therein).
815
816 The changes in the morpho-sedimentary behaviour of these internally drained playa-
817 lakes depend on the relative contribution of the processes that lead to accumulation of
818 sediments in the lake bottom and those that cause its deepening. The processes that
819 determine the complex mass balance in these basins are largely controlled by the

820 presence of evaporite bedrock, groundwater flows that discharge in the lakes and strong
821 winds with great geomorphic effectiveness, as reveals the presence of yardangs.
822
823 Vertical accretion in the lakes may be related to two main types of sedimentary
824 processes: (1) Autochtonous deposition related to evaporitic precipitation of salts from
825 solutes largely supplied by groundwater flow. (2) Allochtonous deposition of extraclasts
826 transported by surface runoff and the wind. La Playa and El Pueyo terminal lakes,
827 covering 1.86 km^2, act as the ultimate sediment sinks for their catchment area of about
828 35 km^2. Additionally, air currents may undergo a reduction in velocity below the
829 transport threshold due to flow separation in these topographic depressions, leading to
830 accumulation of wind-transported particles.
831
832 Deepening of the playa-lakes may be caused by two processes: (1) Groundwater flows
833 that discharge in the lakes may cause dissolution of the bedrock with the consequent
834 subsidence of the lake bottom. This process, albeit continuous, acts at a low rate, since
835 the highly mineralized underground water that discharges in the lakes has a limited
836 karstification capability. (2) Eolian deflation by winds with velocities higher than the
837 entrainment threshold. This process can only operate when the surface of the playa is
838 vegetation free and dry and there is material susceptible to be entrained by air currents.
839 Several processes such as drying cycles, salt weathering, trampling and biogenic
840 burrowing predispose particles to wind erosion (i.e. Goudie and Wells, 1995). Lowering
841 of the lake bottom by eolian deflation is limited by the position of the water table and
842 the capillary fringe (elevation to which the groundwater ascends by capillary force),
843 controlling the development of extremely flat surfaces (Stokes, 1968; Rosen, 1994;
844 Yechieli and Wood, 2002). Once the surface meets the water table, the basins cannot get

any deeper, but expand laterally through backward retreat of their margins. According to Rosen (1994), in order to have net aggradation in a playa, the surface must be flooded more often than it is dry.

The relative contribution of the processes listed above may be significantly altered by climate and land use changes. Under more arid conditions the playas remain dry during longer periods, favouring the lowering of the surface by deflation. Conversely, lower water availability in the semiarid areas may involve a significant reduction in the vegetation cover, with the consequent increase in sediment flux by runoff and deflation; that is higher detrital input to the terminal lakes (Knox, 1984; Bull, 1991). A similar impact may be expected from anthropogenic reductions in the vegetation cover (deforestation, fires, overgrazing). On the contrary, a denser vegetation cover and more frequent flooding under a relatively more humid climate would hinder both external detrital input and eolian deflation. A wetter climate would also favour dissolution-induced subsidence. According to this conceptual model, a change to drier conditions could lead to net erosion or aggradation depending on the relative role of the different processes on the mass balance, mainly deflation *vs* external detrital input. However, it is widely accepted that major deepening phases in playa-lakes and pans occur during more arid periods, when the bottom of the depressions is exposed more frequently to wind deflation and the conditions are more favourable to the preparation of wind-exportable particles (i.e. Goudie and Wells, 1995; Gutiérrez-Elorza et al., 2005; Washington et al., 2006). This is also our preferred interpretation for the studied lakes based on the following circumstances: (1) The middle terrace records the existence of a single lake 47% larger than the present-day La Playa and El Pueyo playas, suggesting a more positive hydrological budget. (2) Although La Playa-El Pueyo lake basin has a large

870 catchment area, the connectivity (coupling) between the slopes, drainage network and
871 terminal lakes is rather limited due to the dominantly flat topography of the platform,
872 dissected by poorly ranged valleys with low topographic gradient (Fig. 4). Higher
873 sediment yield from the slopes could involve increased aggradation in the valleys but
874 limited sediment transfer to the lakes. (3) Runoff has a very limited efficiency within
875 the lakes due to the extremely flat topography, hindering sediment redistribution from
876 the margins towards the centre.
877
878 A number of publications present chronological information on Holocene aggradation
879 and incision phases in ephemeral valleys within the Ebro Depression (Fig. 13). The
880 variable chronologies suggests considerable spatial variations in the timing of the
881 aggradation/incision sequences, most probably related to the superposition of climatic
882 and local factors (human activity, extreme hydrological events, local base level changes
883 and hillslope-channel coupling conditions; i.e. Constante et al., 2010) on the response of
884 these highly sensitive systems. The available data indicates that during the period of
885 accumulation of the middle lacustrine terrace, some ephemeral fluvial systems were
886 dominated by both aggradation and incision processes. There seems to be a temporal
887 cluster of aggradation phases (2.4-1.8 ka BP) correlative to the uppermost part of the
888 middle terrace.
889
890 A recent generation of talus flatirons has been AMS ^{14}C dated at three sites in the Ebro
891 Depression, recording an accumulation phase in the slopes between 3-2.5 ka BP. This
892 aggradation period in the slopes, contemporaneous with the lower half of the lake
893 terrace, is attributed to warm/wet conditions that favoured an increase in the vegetation
894 cover preventing incision in the slopes (Gutiérrez-Elorza et al., 2010). This

895 interpretation is in agreement with a more positive hydrological budget in the lakes,
896 with more frequent flooding preventing deflation. The aggradation period recorded by
897 the middle terrace of La Playa partially overlaps with a phase of increased frequency of
898 large magnitude floods inferred from slackwater flood deposits (2880-2430 cal yr BP)
899 and a cluster of dates from alluvial floodplain deposits (2750-2150 cal yr BP) identified
900 by Thorndycraft and Benito (2006) in Spain.
901
902 The onset of the Mid Holocene period of higher aridity in the Iberian Peninsula at
903 around 6 ka BP correlates with decreasing moisture in the Alps (Magny 2006) and the
904 end of the African Humid Period in northern Africa (Kropelin et al. 2008), and it has
905 been interpreted as a reflection of decreasing summer solar radiation in the northern
906 hemisphere. The 4.2 ka arid event has been characterized in eastern (Weiss et al., 1993;
907 Arz et al., 2006), central (Drysdale et al., 2006, Magny et al., 2007) and western regions
908 (Martín-Puertas et al., 2009) as a period of intense droughts in the Mediterranean that
909 ended the long Mid Holocene arid period and inaugurated the relatively more humid
910 late Holocene.
911
912 The review of available lacustrine, pollen and archaeological records in the Central
913 Ebro valley by González-Sampériz et al (2008) identified the early Holocene as the
914 more humid period during the Holocene, contrasting with the arididy of the Middle
915 Holocene interval, and a moisture recovery during the late Holocene. Mid Holocene
916 deposits are frequently absent in the Central Ebro valley lakes as a result of intense
917 eolian erosive processes. The lack of archaeological remains associated with the Middle
918 Holocene (Neolithic) also supports increased aridity that would have impeded human
919 settlements. Palynological sequences from archaeological and lacustrine sites in

920 northeastern Spain have documented significant changes in vegetation during the last
921 millennia, although in most cases they have been ascribed to human impact more than
922 to climate or hydrological changes. A list of the most significant pollen sites in NE
923 Spain includes: Cova Punta Farisa (Burjachs, 1993), Majaladares Cave (López-García,
924 1992), Salada Mediana (Valero-Garcés et al., 2000a), Laguna Guallar (Davis, 1994), La
925 Clota, El Rebollón and El Camerón (Pérez-Obiol and Roure, 1990), La Playa and La
926 Salineta (González-Sampériz et al., 2008), Salada Pequeña and La Estanca (Davis,
927 1994), Gallocanta (Davis, 1994; Burjachs et al., 1996; Roc et al., 2002), Tozal de
928 Macarullo, Tozal de Andrés and El Prao (González-Sampériz and Sopena, 2002),
929 Taravilla Lake (Moreno et al., 2008), Cabezo de la Cruz (Iriarte, 2009), Estanya Lake
930 (Morellón et al., 2011) or El Cabo and La Cabañeta (González-Sampériz, 2004) sites,
931 among others. Although the chronological resolution is different for these records, all of
932 them show a recent period characterized by: i) less arboreal pollen content (AP)
933 dominated by pines, some junipers and evergreen oaks, interpreted as a result of
934 deforestation processes; ii) the beginning of continuous curves of *Olea*, *Ceralia* and/or
935 *Vitis* and the presence of isolated grains of *Castanea* or *Juglans,* showing the
936 development of cultivated areas; iii) the increase of nitrophilous and herbaceous taxa,
937 frequently related to pastoralism and agricultural activities (Brassicaceae,
938 Cichorioideae, Asteroideae, *Plantago, Rumex,* Chenopodiaceae, etc). Thus, although the
939 main patterns of the recent Holocene vegetation landscape evolution at a regional scale
940 are known, the investigated sequences lack sufficient chronological and geographical
941 resolution to reconstruct a more precise palaeoclimatic scenario for the last millennia.
942
943 Large paleohydrological fluctuations during the last 4 ka have been described in
944 numerous sequences in the Iberian Peninsula. Lacustrine (e.g., Zoñar Lake (Martín-

945 Puertas et al. 2008), Taravilla Lake (Moreno et al. 2008), Estanya Lake (Morellón et al.
946 2009), Redon Lake (Plá and Catalán, 2005), marine (Frigola et al., 2007; Martín–
947 Puertas et al., 2010) and fluvial records (Thorndycraft and Benito, 2006) document a
948 large regional climate variability and millennial scale moisture fluctuations, particularly
949 the mid Holocene arid period with the 4 ka BP crisis, the cold Iron Ages followed by
950 the Iberian-Roman Humid Period, and the dry and warm Medieval Climate Anomaly
951 (Moreno et al., 2011, 2012; Morellón et al., 2012). At a millennial scale, the playa-lake
952 records in the Central Ebro Basin have shown the occurrence of an arid period prior to 4
953 ka and a recovery of average saline lake levels during the last millennia (Valero-Garcés
954 et al., 2000a, b, c, 2004; González-Sampériz et al., 2008). But, as we have described
955 above, the large paleohydrological variability during the Late Holocene detected in
956 other Mediterranean and Iberian regions has not been identified in the Central Ebro
957 Basin lake sequences because they do not have the adequate chronological resolution.
958
959 Both, La Playa middle terrace and La Salineta terrace document large paleohydrological
960 fluctuations in the lake basins with intense and very significant periods of aggradation
961 and excavation during the last 4000 years. However, the correlation between both
962 sequences is not possible due to the absence of a more constrained chronological
963 framework for La Salineta terrace. The occurrence of an aggradation phase in La Playa
964 lake after 3.9 ka is coherent with a number of Iberian and Mediterranean records that
965 show more humid conditions after the 4.2 ka event. In Montcortès lake (Lleida, NE
966 Spain), an humidity increase occurred between 3800-2350 cal yr BP (Corella et al., in
967 press), similar to that at Zoñar Lake (Córdoba, S Spain) after 3.5 ka (Martín-Puertas et
968 al. 2008, 2009). This period corresponds with the cold and wet phase of the Iron Age in
969 northern Europe (Leira, 2005) between 3000 and 2000 cal yr BP (1050-50 BC), marked

970 humid conditions in some alpine lakes (Magny et al., 2007) between 3950–3850 cal yr
971 BP, the onset of the humidity increase in the Mediterranean area (Sadori et al., 2004)
972 and evidence of higher flood activity (2865-2350 cal yr BP) in the Spanish fluvial
973 record (Thorndycraft and Benito, 2006). This period includes the Bronze Age (4-2.7 ka
974 BP) and the first part of the Iron Age, when several areas of the Ebro Depression show
975 an intense occupation pattern (some caves but more frequently open sites in lowlands
976 and middle altitudes) and therefore, a high population density (Utrilla and Rodanés,
977 1997), probably in response to a more humid period.
978
979 The erosional phase that occurred after ca. 2 ka is coherent with relatively more arid
980 conditions in the Iberian Peninsula after the Roman Period and also during the Medieval
981 Ages (Moreno et al., 2011, 2012): in Lake Montcortès, a lake level drop between 2350
982 and 1910 cal yr BP (400 BC - 40 AD) has been inferred by Corella et al (2011)
983 coinciding with a reduction in river flood frequency on the Iberian Peninsula between
984 2350 and 2000 cal yr BP (Macklin et al., 2006) and lower lake levels in Zoñar Lake
985 between 2,100 and 1,900 cal yr BP (Martín-Puertas et al., 2008).
986
987
988 **Acknowledgements**
989 This research work has been funded by the national projects CGL2005-02404,
990 CGL2010-16775 (Ministerio de Ciencia e Innovación and FEDER), CGL2009-07992
991 (DINAMO), CGL2009-08415 (GLOBALKARST) and the GRACCIE-CONSOLIDER
992 INGENIO 2010 (CSD2007-00067). A. Moreno acknowledges the “Ramón y Cajal”
993 postdoctoral program for funding. P. Lucha has been supported by a postdoctoral grant
994 of the Spanish Ministry of Education. We are thankful to Jaime Bonachea, Mario

995 Morellón, Laia Casadellà and Agustí Rodríguez for their help in the field. We are very
996 grateful to Dr. Carmen Castañeda and Dr. Yehouda Enzel for their careful and valuable
997 reviews.

998 **References**

999

1000 Adamiec, G., Aitken, M.J., 1998. Dose rate conversion factors: update. Ancient TL 8,
1001 12-14.
1002 Aguilella, A., Riera, J., 1997. Estudios sobre la vegetación y flora halófilas de las
1003 saladas de "El Plano" (Alcañiz-Calanda, Aragón, España). In: Anento, J.L., Selfa, J.,
1004 Jiménez, R. (Eds.). Las saladas de Alcañiz. Estudio Multidisciplinar Serie
1005 Investigación. Publicaciones del Consejo de Protección de la Naturaleza de Aragón,
1006 Zaragoza, pp. 43-100.
1007 Aitken, M.J., 1985. Thermoluminescence Dating. Academic Press, London, 359 pp.
1008 Aitken, M., 1998. An Introduction to Optical Dating. Oxford University Press, Oxford,
1009 267 pp.
1010 Anderson, R.Y., Allen, B.D., Menking, K.M., 2002. Geomorphic expression of abrupt
1011 climate change in southwestern North America at the glacial termination.
1012 Quaternary Research 57, 371-381.
1013 Aramburu, P., 1904. Las saladas de Sátago. Boletín de la Real Sociedad Española de
1014 Historia Natural 4, 428-429.
1015 Arauzo-García, T., Gutiérrez-Elorza, M., 1994. Evolución de los valles de fondo plano
1016 del centro de la Depresión del Ebro. In: Arnáez-Vadillo, J., García-Ruiz, J.M.,
1017 Gómez-Villar, A. (Eds.), Geomorfología en España. III Reunión de Geomorfología,
1018 Vol. 1, pp. 277-290.
1019 Arlegui, L.E., 1996. Diaclasas, fallas y campo de esfuerzos en el sector central de la
1020 Cuenca del Ebro. Ph. D. Thesis. University of Zaragoza, 308 pp.
1021 Arnold, L.J., Roberts, R.G. 2011. Paper I – Optically stimulated luminescence (OSL)
1022 dating of perennially frozen deposits in north-central Siberia: OSL characteristics of

quartz grains and methodological considerations regarding their suitability for dating. Boreas, 40, 389-416.

Arnold, L.J., Roberts, R.G., Galbraith, R.F., DeLong, S.B., 2009. A revised burial dose estimation procedure for optical dating of young and modern-age sediments. Quaternary Geochronology 4, 306-325.

Arnold, L. J., Roberts, R. G., MacPhee, R. D. E., Haile, J. S., Brock, F., Möller, P., Froese, D. G., Tikhonov, A. N., Chivas, A. R., Gilbert, M. T. P., Willerslev, E. 2011. Paper II – Dirt, dates and DNA: OSL and radiocarbon chronologies of perennially frozen sediments in Siberia and their implications for sedimentary ancient DNA studies. Boreas 40, 417-445.

Arnold, L.J., Duval, M., Falguères, C., Bahain, J.-J., Demuro, M. 2012. Portable gamma spectrometry with cerium-doped lanthanum bromide scintillators: Suitability assessments for luminescence and electron spin resonance dating applications. Radiation Measurements 47, 6-18.

Arz, H.W., Lamy, F., Patzold, J., 2006. A pronounced dry event recorded around 4.2 ka in brine sediments from the northern Red Sea. Quaternary Research 66, 432-441.

Ascaso, A., Cuadrat, J.M., 1981. El clima. In: Higueras, A. (Ed.), Geografía de Aragón. Guara, Zaragoza, pp. 93-140.

Balsa, J., Pascual, M.L., Guerrero, M.C., Montes, C., 1991. Las saladas de Bujaraloz-Sátago y la Salada de Chiprana: Riqueza natural de Aragón. Empelte 7, 3-30.

Bauer, P., Supper, R., Zimmermann, S., Kinzelbach, W., 2006. Geoelectrical imaging of groundwater salinization in the Okavango Delta, Botswana. Journal of Applied Geophysics 60, 126–141.

Beck, B.F., 2005. Soil piping and sinkhole failures. In: Culver, D.C., White, W.B. (Eds.), Enyclopedia of Caves. Elsevier, New York, pp. 523-528.

1048 Bell, F.G., 2007. Engineering Geology. Elsevier. Amsterdam, 581pp.
1049 Bowler, J.M., Johnston, H., Olley, J.M., Prescott, J.R., Roberts, R.G., Shawcross, W.,
1050 Spooner, N.A., 2003. New ages for human occupation and climatic change at Lake
1051 Mungo, Australia. Nature 421, 837-840.
1052 Boyé, M., Marmier, F., Nelson, C., Trécolle, G., 1978. Le dépots de la Sebka Mellala.
1053 Revue de Géomorphologie Dynamique 27, 49-62.
1054 Brakenridge, G.R., 1985. Rate estimates for lateral bedrock erosion based on
1055 radiocarbon ages, Duck River, Tennessee. Geology 13, 111-114.
1056 Braun-Blanquet, J., de Bolòs, O., 1957. Les groupements végétaux du bassin moyen de
1057 l'Ebre et leur dynamisme. Anales de la Estación Experimental de Aula Dei,
1058 Zaragoza, Vol. 5, 266 pp.
1059 Brennan, B.J., 2003. Beta doses to spherical grains. Radiation Measurements 37, 299-
1060 303.
1061 Bull, W.B., 1991. Geomorphic responses to climate change. Oxford University Press.
1062 Oxford, 326 pp.
1063 Burillo, F., Gutiérrez-Elorza, M., Peña-Monné, J.L., 1985. Las acumulaciones
1064 holocenas y su datación arqueológica en Mediana de Aragón (Zaragoza). Cuadernos
1065 de Investigación Geográfica 11, 193-207.
1066 Burjachs, F., 1993. Anàlisi paleopalinològica del jaciment arqueològic de la Cova
1067 Farisa. Estudios de la Antigüedad 6/7. Universidad Autónoma de Barcelona, pp. 41-
1068 43.
1069 Burjachs, F., Rodó, X., Comín, F.A., 1996. Gallocanta: ejemplo de secuencia
1070 palinológica en una laguna efímera. In: Ruiz Zapata, B. (ed.) Estudios
1071 Palinológicos, XI Simposio de Palinología, Universidad de Alcalá, pp. 25-29.

1072 Cassiani, G., Bruno, V., Villa, A., Fusi, N., Binley, A.M., 2006. A saline trace test
1073 monitored via time-lapse surface electrical resistivity tomography. Journal of
1074 Applied Geophysics 59, 244–259.
1075 Castañeda, C., 2002. El agua de las saladas de Monegros sur estudiada con datos de
1076 campo y de satélite. Gobierno de Aragón. Publicación del Consejo de Protección de
1077 la Naturaleza 35, Zaragoza, 158 pp.
1078 Castañeda, C., Herrero, J., Casterad, M.A., 2005. Facies identification within the playa-
1079 lake of the Monegros desert, Spain, from field and satellite data. Catena 63, 39-63.
1080 Cooke, R., Warren, A., Goudie, A., 1993. Desert Geomorphology. UCL Press, London,
1081 526 pp.
1082 Constante, A., Peña, J.L., Muñoz, A., Picazo, J., 2010. Climate and anthropogenic
1083 factors affecting alluvial fan development during the late Holocene in the central
1084 Ebro Valley, northeast Spain. The Holocene 21, 275-286.
1085 Corella, P., Moreno, A., Morellón, M., Rull, V., Giralt, S., Rico, M, Sanz-Pérez, A.,
1086 Valero-Garcés, B. (in press) Sedimentary evolution and palaeohydrology of karstic,
1087 meromictic Montcortés Lake (Spanish Pre-Pyrenees) during the last 6,000 years.
1088 Journal of Paleolimnology DOI 10.1007/s10933-010-9443-3.
1089 Cuchí, J.A., Soriano, M.A., 1991. The Val of San Marcos. Study of an infilled valley in
1090 the Ebro Basin. University of Zaragoza. Unpublished report.
1091 Davis, B.A.S., 1994. Paleolimnology and Holocene environmental change from
1092 endorheic lakes in the Ebro Basin, north-east Spain. Ph.D. Thesis. University of
1093 Newcastle upon Tyne, UK.
1094 Davis, B.A.S., Brewer, S., Stevenson, A.C., Guiot, J., Data Contributors, 2003. The
1095 temperature of Europe during the Holocene reconstructed from pollen data.
1096 Quaternary Science Reviews 22, 1701-1716.

1097 Desir, G., Gutiérrez-Elorza, M., Gutiérrez-Santolalla, F., Marín, C., 2011. Las formas y
1098 depósitos eólicos de la Depresión del Ebro. In: Sanjaume, E., Gracia, F.J., Flor, G.
1099 (Eds.), Las dunas en España. Sociedad Española de Geomorfología, 16 pp.
1100 Drysdale, R., Zanchetta, G., Hellstrom, J., Maas, R., Fallick, A., Pickett, M., Cartwright,
1101 I., Piccini, L., 2006. Late Holocene drought responsible for the collapse of Old
1102 World civilizations is recorded in an Italian cave flowstone. Geology 34, 101-104.
1103 Dupré, M., 1992. Palinología. Cuadernos Técnicos de la Sociedad Española de
1104 Geomorfología 5, 1-30.
1105 Frigola, J., Moreno, A., Cacho, I., Canals, M., Sierro, F. J., Flores, J.A., Grimalt, J.O.,
1106 Hodell, D.A., Curtis, J.H., 2007. Holocene climate variability in the western
1107 Mediterranean region from a deepwater sediment record. Paleoceanography 22
1108 PA2209, 16 pp.
1109 Galbraith, R.F., Roberts, R.G., Laslett, G.M., Yoshida, H., Olley, J.M., 1999. Optical
1110 dating of single and multiple grains of quartz from Jinmium rock shelter, northern
1111 Australia: Part I, experimental design and statistical models. Archaeometry 41, 339-
1112 364.
1113 García-Vera, M.A., 1996. Hidrogeología de zonas endorreicas en climas semiáridos.
1114 Aplicación a Los Monegros (Zaragoza y Huesca). Diputación General de Aragón,
1115 Zaragoza, 297 pp.
1116 González-Sampériz, P., 2004. Evolución paleoambiental del sector central de la cuenca
1117 del Ebro durante el Pleistoceno superior y Holoceno. Instituto Pirenaico de
1118 Ecología-CSIC, Zaragoza, 210 pp.
1119 González-Sampériz, P., Sopena, M.C., 2002. Recent Holocene palaeoenvironmental
1120 evolution in the Central Ebro Basin (NE Spain). Quaternary International 93-94,
1121 177-190.

González-Sampériz, P., Valero-Garcés, B.L., Moreno, A., Morellón, M., Navas, A., Machín, J., Delgado-Huertas, A., 2008. Vegetation changes and hydrological fluctuations in the Central Ebro Basin (NE Spain) since the Late Glacial period: Saline lake records. Paleogeography, Paleoclimatology, Paleoecology 259, 157-181.

Goudie, A.S., 2007. Mega-yardangs: a global analysis. Geography Compass 1, 65-81.

Goudie, A.S., Wells, G.L., 1995. The nature, distribution and formation of pans in arid zones. Earth-Science Reviews 38, 1-69.

Goudie, A., Stokes, S., Cook, J., Samieh, S., El-Rashidi, O.A., 1999. Yardang landforms from Kharga Oasis, south-western Egypt. Zeitschrift für Geomorphologie supplementband 116, 97-112.

Griffiths, D.H., Barker, R.D., 1993. Two-dimensional resistivity imaging and modelling in areas of complex geology. Journal of Applied Geophysics 29, 211-226.

Gutiérrez-Elorza, M., Desir, G., Gutiérrez-Santolalla, F., 2002. Yardangs in the semiarid central sector of the Ebro Depression (NE Spain). Geomorphology 44, 155-170.

Gutiérrez-Elorza, M., Desir, G., Gutiérrez, F., Marín, C., 2005. Origin and evolution of playas and blowouts in the semiarid zone of Tierra de Pinares (Duero Basin, Spain). Geomorphology 73, 50-63.

Gutiérrez-Elorza, M., Lucha, P., Gutiérrez, F., Moreno, A., Guerrero, J., Martín-Serrano, A., Nozal, F., Desir, G., Marín, G., Bonachea, J., 2010. Are talus flatiron sequences in Spain climate-controlled landforms?. Zeitschrift für Geomorphologie 54, 2, 243-252.

Gutiérrez, F., Arauzo, T., 1995. Fenómenos recientes de subsidencia kárstica sinsedimentaria en el Barranco de Torrecilla (Depresión del Ebro, Zaragoza). Cuaternario y Geomorfología 9 (1-2), 73-90.

1147 Gutiérrez, F., Cooper, A.H., 2011. Surface morphology of gypsum karst. In: Frumkin,
1148 A. (Ed.). Treatise on Geomorphology. Elsevier. In press.
1149 Gutiérrez, F., Guerrero, J., Lucha, P., 2008a. A genetic classification of sinkholes
1150 illustrated from evaporite paleokarst exposures in Spain. Environmental Geology
1151 53, 993-1006.
1152 Gutiérrez, F., Ortuño, M., Lucha, P., Guerrero, J., Acosta, E., Coratza, P., Piacentini, D.,
1153 Soldati, M., 2008b. Late Quaternary episodic displacement on a sackung scarp in
1154 the central Spanish Pyrenees. Secondary paleoseismic evidence?. Geodinámica Acta
1155 21, 187-202.
1156 Gutiérrez, F., Galve, J.P., Lucha, P., Bonachea, J., Jordá, L., Jordá, R., 2009.
1157 Investigation of a large collapse sinkhole affecting a multi-storey building by means
1158 of geophysics and the trenching technique (Zaragoza city, NE Spain).
1159 Environmental Geology 58, 1107-1122.
1160 Gutiérrez, F., Lucha, P., Galve, J.P., 2010. Reconstructing the geochronological
1161 evolution of large landslides by means of the trenching technique in the Yesa
1162 Reservoir (Spanish Pyrenees). Geomorphology 124, 124-136.
1163 Harrison, S.P., Yu, G., Tarasov, P.E., 1996. The Holocene lake levels record from
1164 Eurasia. Quaternary Research 45, 138-159.
1165 Harvey, A.M., Gutiérrez-Elorza, M., 2005. Repeated patterns of Quaternary
1166 discontinuous gullying at El Tormillo, Ebro Basin. In: García, C. and Batalla, R.J.
1167 (Eds.). Catchment Dynamics and River Processes: Mediterranean and Other Climate
1168 Regions. Elsevier. Amsterdam, pp. 53-67.
1169 Hetch, S., 2003. Investigation of the shallow subsurface with seismic refraction
1170 methods. Application potentials and limitations with examples from various field
1171 studies. Zeitschrift für Geomorphologie. N.F., Supplementband 132, 19-36

1172 Hoffmann, T., Schrott, L., 2003. Determining sediment thickness of talus slopes and
1173 valley fill deposits using seismic refraction – a comparison of 2D interpretation
1174 tools. Zeitschrift für Geomorphologie. N.F., Supplementband 132, 71-87.
1175 Ibáñez, M.J., 1975. El endorreismo del sector central de la depresión del Ebro.
1176 Cuadernos de Investigación Geográfica 1, 35-48.
1177 Iriarte, M.J., 2009. Los inicios del Holoceno Reciente en el valle del río Huerva: la
1178 secuencia palinológica protohistórica del cabezo de la Cruz. In: Picazo, J., Rodanés,
1179 J.M. (Eds.), Cabeza de la Cruz, La Muela, Zaragoza. Los poblados del Bronce Final
1180 y Primera Edad del Hierro. Gobierno de Aragón, Zaragoza, pp. 108-131.
1181 IRYDA, 1989. Estudio geohidrológico de las Sectores VIII, IX y XI de la zona regable
1182 de Monegros II (Zaragoza y Huesca). Madrid, unpublished report.
1183 Knox, J.C., 1984. Fluvial responses to small scale climate changes. In: Costa, G.E.,
1184 Fleisher, P.J. (Eds.), Developments and Applications of Geomorphology. Springer
1185 Verlag, Berlin, pp. 318– 342.
1186 Kropelin, S., Verschuren, D., Lezine, A. M., Eggermont, H., Cocquyt, C., Francus, P.,
1187 Cazet, J. P., Fagot, M., Rumes, B., Russell, J. M., Darius, F., Conley, D.J., Schuster,
1188 M., von Suchodoletz, H. and Engstrom, D. R. 2008 Climate-Driven Ecosystem
1189 Succession in the Sahara: The Past 6000 Years. Science 320, 765-768
1190 Leira, M., 2005. Diatom responses to Holocene environmental changes in a small lake
1191 in northwest Spain. Quaternary International 140-141, 90-102.
1192 Liso, M., Ascaso, A., 1969. Introducción al estudio de la evapotranspiración y
1193 clasificación climática de la Cuenca del Ebro. An. Estac. Exp. Aula Dei, C.S.I.C. 10
1194 Zaragoza, 505 pp.
1195 Leroux, V., Dahlin, T., 2006. Time-lapse resistivity investigations for imaging saltwater
1196 transport in glaciofluvial deposits. Environmental Geology 49, 347–358.

1197 Liu, D., Abuduwaili, J., Lei, J., Wu, G., Gui, D. 2011. Wind erosion of saline playa
1198 sediments and its ecological effects in Ebinur Lake, Xinjiang, China. Environmental
1199 Earth Sciences 63, 241-250.
1200 Loke, M.H., Barker, R.D., 1996. Rapid least-squares inversion of apparent resistivity of
1201 apparent resistivity pseudosections by a quasi-Newton method. Geophysical
1202 Prospecting 44, 131-152 .
1203 Longares, L.A., 1997. El paisaje vegetal en el entorno de la Reserva Ornitológica "El
1204 Planerón" (Belchite, Zaragoza). Consejo de Protección de la Naturaleza-
1205 SEO/Birdlife. Serie Investigación 7, Zaragoza, 195 pp.
1206 López, P.L., Auqué, L., Mandado, J., Vallès, V., Gimeno, M.J., Gómez, J., 1999.
1207 Determinación de la secuencia de precipitación salina en la Laguna La Playa
1208 (Zaragoza, España). I. Condiciones de equilibrio mineral y simulación teórica del
1209 proceso. Revista de la Sociedad Geológica de España 55, 27-44.
1210 López-García, P., 1992. Análisis polínicos de cuatro yacimientos arqueológicos situados
1211 en el Bajo Aragón. Aragón / Litoral Mediterráneo. Intercambios culturales durante
1212 la Prehistoria. Institución Fernando el Católico. Universidad de Zaragoza. Zaragoza,
1213 pp. 235-242.
1214 Macklin, M.G., Passmore, D.G., Stevenson, A.C., Davis, B.A., 1994. Responses of
1215 rivers and lakes to Holocene environmental change in the Alcañiz region, Teruel,
1216 North-East Spain. In: Millington, A.C. and Pye, K. (Eds.), Environmental Change in
1217 Drylands: Biogeographical and Geomorphological Perspectives. John Wiley and
1218 Sons, pp. 113-130.
1219 Macklin, M.G., Benito, G., Gregory, K.J., Johnstone, E., Lewin, J., Michczyńska, D.J.,
1220 Soja, R., Starkel, L., Thorndycraft, V.R., 2006. Past hydrological events reflected in
1221 the Holocene fluvial record of Europe. Catena 66, 145–154.

1222 Magny, M., de Beaulieu, J.-L., Drescher-Schneider, R., Vannière, B., Walter-Simonnet,
1223 A.-V., Millet, L., Bossuet, G., Peyron, O., 2006. Climatic oscillations in central
1224 Italy during the Last Glacial-Holocene transition: the record from Lake Accesa.
1225 Journal of Quaternary Science 21, 311-320.
1226 Magny, M., de Beaulieu, J. -L., Drescher-Schneider, R., Vannière, B., Walter-Simonnet,
1227 A. -V., Miras, Y., Millet, L., Bossuet, G., Peyron, O., Brugiapaglia, E. and Leroux,
1228 A. 2007. Holocene climate changes in the central Mediterranean as recorded by
1229 lake-level fluctuations at Lake Accesa (Tuscany, Italy). Quaternary Science Review
1230 26, 1736-1758.
1231 Mahan, S.A., Noe, D.C., McCalpin, J.P., 2009. Use of OSL dating to establish the
1232 stratigraphic framework of Quaternary eolian sediments, Anton scarp upper trench,
1233 Northeastern Colorado High Plains, USA. Quaternary International 199, 92-103.
1234 Martín-Puertas, C., Valero-Garcés, B., Mata, P., González-Sampériz, P., Bao, R.,
1235 Moreno, A., Stefanova, V., 2008. Arid and humid phases in southern Spain during
1236 the last 4000 years: The Zoñar Lake record, Córdoba. Holocene 18, 907–921.
1237 Martín-Puertas, C., Valero-Garcés, B., Brauer, A., Mata, P., Delgado-Huertas, A.,
1238 Dulski, P., 2009. The Iberian–Roman Humid Period (2600–1600 cal yr BP) in the
1239 Zoñar Lake varve record (Andalucía, southern Spain). Quaternary Research 71, 108-
1240 120.
1241 Martín-Puertas, C., Jiménez-Espejo, F., Martínez-Ruiz, F., Nieto-Moreno, V., Rodrigo,
1242 M., Mata, P., Valero-Garcés, B., 2010. Late Holocene climate variability in the
1243 southwestern Mediterranean region: an integrated marine and terrestrial
1244 geochemical approach. Climate of the Past Discussions 6, 1655-1683.
1245 Mees, F., Castañeda, C., Van Ranst, E., 2011. Sedimentary and diagenetic features in
1246 saline lake deposits of the Monegros region, northern Spain. Catena 85, 245-252.

1247 McCalpin, J.P., 2009. Field techniques in Paleoseismology. Terrestrial environments.
1248 In: McCalpin, J.P. (Ed.), Paleoseismology. Academic Press, San Diego, pp. 29-118.
1249 McCalpin, J.P., 2011. Trenching and exposed faces. Treatise of Geomorphology.
1250 Elsevier. In press.
1251 McCauley, J., Grolier, M., Breed, C., 1977. Yardangs of Peru and other desert regions.
1252 USGS Interagency Rep., Astrogeology 81, 177 pp.
1253 Mejdahl, V., 1979. Thermoluminescence dating: beta-dose attenuation in quartz grains.
1254 Archaeometry 21, 61-72.
1255 Mingarro, F., Ordóñez, S., López de Azcona, M.C., García del Cura, M.A., 1981.
1256 Sedimentoquímica de las lagunas de los Monegros y su entrono geológico. Boletín
1257 Geológico y Minero 92-93, 171-195.
1258 Molero, J., Blanché i Vergés, C., 1986. Las cubetas arreicas al sur de Bujaraloz (Valle
1259 del Ebro). Contribución a su estudio fitocenológico. Lazaroa 9, 277-300.
1260 Morellón, M., Valero-Garcés, B., Vegas, T., González-Sampériz, P., Delgado-Huertas,
1261 A., Mata, P., Moreno, A., Rico, M., Corella, J.P. 2009. Late glacial and Holocene
1262 palaeohydrology in the western Mediterranean region: the Lake Estanya record (NE
1263 Spain) Quaternary Science Reviews 28, 2582–2599.
1264 Morellón, M., Valero-Garcés, B., González-Sampériz, P., Vegas-Villarúbia, T., Rubio,
1265 E., Rieradevall, M., Delgado-Huertas, A., Mata, P., Romero, O., Engstrom, D.R.,
1266 López-Vicente, M., Navas, A., Soto, J. (2011) Climate changes and human impact
1267 recorded in the sediments of Lake Estanya (NE Spain) during the Medieval Warm
1268 Period and Little Ice Age. Journal of Paleolimnology 46, 423–452.
1269 Morellón, M., Pérez-Sanz, A., Corella, J.P, Büntgen, U., Catalán, J., González-
1270 Sampériz, P., González-Trueba, J.J., López-Sáez, J.A., Moreno, A., Pla, S., Saz-
1271 Sánchez, M.A., Scussolini., P., Serrano, E., Steinhilber, F., Stefanova, V., Vegas-

1272 Vilarrúbia, T., Valero-Garcés, B (2012). A multi-proxy perspective on millennium-
1273 long climate variability in the Southern Pyrenees. Climate of the Past, in press.
1274 Moreno, A., Valero-Garcés, B.L., González-Sampériz, P., Navas, A., Machín, J.,
1275 Delgado-Huetas, A., 2004. El registro paleoambiental y paleoclimático de las
1276 saladas de la Playa y la Salineta (Zona Central de la Depresión del Ebro). Geotemas
1277 6, 137-140.
1278 Moreno, A., Valero-Garcés, B., González-Sampériz, P., Rico, M., 2008. Flood response
1279 to rainfall variability during the last 2000 years inferred from the Taravilla Lake
1280 record (Central Iberian Range, Spain). Journal of Paleolimnology 40, 943–961.
1281 Moreno, A., Morellón, M., Martín-Puertas, C., Frigola, J., Canals, M., Cacho, I.,
1282 Corella, J. P., Pérez, A., Belmonte, A., Vegas-Vilarrúbia, T., González-Sampériz,
1283 P., Valero-Garcés., B., 2011. Was there a common hydrological pattern in the
1284 Iberian Peninsula region during the Medieval Climate Anomaly?. PAGES news, 19,
1285 16-18.
1286 Moreno, A., Pérez, J., Frigola, V., Nieto, M., González-Sampériz, P., Morellón, M.,
1287 Martín-Puertas, C., Corella, J.P., Belmonte, A., Cacho, I., Canals, M., Jiménez-
1288 Espejo, F., Martínez Ruiz, F., Vegas, T., Valero-Garcés, B. (2012). The Medieval
1289 Climate Anomaly in the Iberian Peninsula reconstructed from marine and lake
1290 records. Quaternary Science Reviews
1291 Peña, J.L., 1996. Los valles holocenos del escarpe en yesos de Juslibol (sector central de
1292 la Depresión del Ebro). Aspectos geomorfológicos y geoarqueológicos. Arqueología
1293 Espacial 15, 83-102.
1294 Peña, J.L., Julián, A., Chueca, J., Echeverría, M.T., Ángeles, G.R., 2004. Etapas de
1295 evolución holocena en el valle del Río Huerva: Geomorfología y geoarqueología. In:
1296 Peña, J.L., Longares, L.A., Sánchez, M. (Eds.), Geografía Física de Aragón:

1297 Aspectos generales y temáticos. Universidad de Zaragoza-Institución Fernando El
1298 Católico, pp. 289-302.
1299 Pérez-Obiol, R., Roure, J.M., 1990. Aportaciones palinológicas para la interpretación de
1300 la evolución reciente del paisaje vegetal de los Monegros. Actas VII Simposio
1301 APLE (1988). Granada, pp. 485-491.
1302 Plá, S., Catalan, J., 2005. Chrysophyte cysts from lake sediments reveal the
1303 submillennial winter/spring climate variability in the northwestern Mediterranean
1304 region throughout the Holocene. Climate Dynamics 24, 263-278.
1305 Prentice, I.C., Harrison, S.P., Jolly, D., Guiot, J., 1998. The climate and biomes of
1306 Europe at 6000 yr BP: comparison of model simulations and pollen-based
1307 reconstructions. Quaternary Science Reviews 17, 659-668.
1308 Poulsen, S.E., Rasmussen, K.E., Christensen, N.B., Christensen, S., 2010. Evaluating
1309 the salinity distribution of a shallow coastal aquifer by vertical multielectrode
1310 profiling (Denmark). Hydrogeology Journal 18, 161–171.
1311 Pueyo, J.J., 1978/79. La precipitación evaporítica actual en las lagunas saladas del área:
1312 Bujaraloz, Sástago, Caspe, Alcañiz y Calanda (provincias de Zaragoza y Teruel).
1313 Revista del Instituto de Investigaciones Geológicas. Diputación Provincial de
1314 Barcelona, 33, 5-56.
1315 Pueyo, J.J., 1980. Procesos diagenéticos observados en las lagunas tipo playa de la zona
1316 Bujaraloz-Alcañiz (provincias de Zaragoza y Teruel). Revista del Institución de
1317 Investigaciones Geológicas. Diputación Provincial de Barcelona, 34, 195-207.
1318 Pueyo, J.J., Inglés, M., 1987. Substrate mineralogy, interstitial brine composition and
1319 diagenetic processes in the playa lakes of Los Monegros and Bajo Aragón (Spain).
1320 In: Rodríguez-Clemente, R., Tardy, Y. (Eds.), Geochemistry and Mineral Formation
1321 in the Earth Surface, pp. 351-372.

1322 Puicercús, J.A., Valero, A., Navarro, J., Terrén, R., Zubiaur, R., Martín, F., Iniesta, G.,
1323 1997. Atlas Eólico de Aragón. Gobierno de Aragón, Zaragoza, 127 pp.
1324 Quirantes, J., 1965. Notas sobre las lagunas de Bujaraloz-Sástago. Geographica 12, 30-
1325 34.
1326 Quirantes, J., 1978. Estudio sedimentológico y estratigráfico del Terciario continental
1327 de los Monegros. Instituto Fernando El Católico, Zaragoza, 200 pp.
1328 Ramírez, J.I., 1997. Mapa Geológico de España a Escala 1:50000. Gelsa (413). Instituto
1329 Tecnológico Geominero de España, Madrid.
1330 Reimer, P.J., Baillie, M.G.L., Bard, E., Bayliss, A., Beck, J.W., Bertrand, C., Blackwell,
1331 P.G., Buck, C.E., Burr, G., Cutler, K.B., Damon, P.E., Edwards, R.L., Fairbanks,
1332 R.G., Friedrich, M., Guilderson, T.P., Hughen, K.A., Kromer, B., McCormac, F.G.,
1333 Manning, S., Bronk Ramsey, C., Reimer, R.W., Remmele, S., Southon, J.R.,
1334 Stuiver, M., Talamo, S., Taylor, F.W., van der Plicht, J., Weyhenmeyer, C.E., 2009.
1335 IntCal09 and Marine09 radiocarbon age calibration curves, 0-50,000 years cal BP.
1336 Radiocarbon 51, 1111-1150.
1337 Roc, A.C., Sánchez-Goñi, M.F., Pérez, A., Alfonso, S., Jouanneau, J.M., Sánchez, J.A.,
1338 2002. Relación entre la evolución sedimentaria de la Laguna de Gallocanta
1339 (Cordillera Ibérica, NE de España) y la historia de la vegetación de su cuenca
1340 durante el Cuaternario Reciente. Journal of Iberian Geology 28, 243-262.
1341 Rodó, X., Baert, E., Comín, F.A., 1997. Variations in seasonal rainfall in Southern
1342 Europe during the present century: relationships with the North Atlantic Oscillations
1343 and the El Niño-Southern Oscillation. Climate Dynamics 13, 275-284.
1344 Rosen M.R., 1994. The importance of groundwater in playas: A review of playa
1345 classifications and the sedimentology and hydrology of playas. In: Rose, M.R. (Ed.),

1346 Paleoclimate and Basin Evolution of Playa Systems. Geological Society of America
1347 Special Paper 289, 1-18.
1348 Sadori, L., Giraudi, C., Petitti, P., Ramrath, A., 2004. Human impact at Lago di
1349 Mezzano (central Italy) during the Bronze Age: a multidisciplinary approach.
1350 Quaternary International 113, 5-17.
1351 Salvany, J.M., García Vera, M.A., Samper, J., 1994. Influencia del sustrato terciario en
1352 el emplazamiento del complejo lagunar de Bujalaroz (Monegros, Cuenca del Ebro).
1353 Actas II Congr. Esp. Terciario. Jaca, pp. 271–274.
1354 Salvany, J.M., García Vera, M.A., Samper, J., 1996. Geología e hidrogeología de la
1355 zona endorreica de Bujaraloz-Sástago (Los Monegros, provincia de Zaragoza y
1356 Huesca). Acta Geológica Hispánica 30, 31– 50.
1357 Samouëlian, A., Cousin, I., Tabbagh, A., Bruand, A., Richard, G., 2005. Electrical
1358 resistivity survey in soil science: a review. Soil Tillage Research 83, 173–193.
1359 Samper-Calvete, F.J., García-Vera, M.A., 1998. Inverse modelling of groundwater flow
1360 in the semiarid evaporitic closed basin of Los Monégros, Spain. Hydrogeology
1361 Journal 6, 33-49.
1362 Samper, F.J., Custodio, E., García-Vera, M.A., 1993. Preliminary isotopic study of
1363 groundwater salinity variations in the closed basin semiarid area of Los Monegros,
1364 Spain. In: International Symposium on Isotopic Techniques in the Study of Past and
1365 Current Environmental Changes in the Hydrosphere and the Atmosphere.
1366 Proceedings of the International Atomic Energy Agency. IAEA-SM-329, 32, 213-
1367 228.
1368 Sánchez-Navarro, J.A., Pérez, A., Coloma, P., Martínez-Gil, F.J., 1998. Combined
1369 effects of groundwater and aeolian processes in the formation of the northernmost

1370 closed saline depressions of Europe, north-east Spain. Hydrological Processes 12,
1371 813-820.
1372 Sancho, C., Peña, J.L., Muñoz, A., Benito, G., McDonald, E., Rhodes, E.J., Longares,
1373 L.A., 2008. Holocene alluvial morphopedosedimentary record and environmental
1374 changes in the Bardenas Reales Natural Park (NE Spain). Catena 73, 225-238.
1375 Schrott, L., Sass, O, 2008. Application of field geophysics in geomorphology: Advances
1376 and limitations exemplified by case studies. Geomorphology 93, 55-73.
1377 Schütt, B., 1998. Reconstruction of paleoenvironmental conditions by investigations of
1378 Holocene playa sediments in the Ebro Basin, Spain: preliminary results.
1379 Geomorphology 23, 273-283.
1380 Scott, J.H., 1973. Seismic refraction modelling by computer. Geophysics 28, 271-284.
1381 Stokes, W.L., 1968. Multiple parallel-truncation bedding planes. A feature of wind
1382 deposited sandstone formation. Journal of Sedimentary Petrology 38, 510-515.
1383 Stokes, S., Ingram, S., Aitken, M. J., Sirocko, F., Anderson, R., Leuschner, D., 2003.
1384 Alternative chronologies for Late Quaternary (Last Interglacial-Holocene) deep sea
1385 sediments via optical dating of silt-sized quartz. Quaternary Science Reviews 22,
1386 925-941.
1387 Sumanovac, F., 2006. Mapping of thin sandy aquifers by using high resolution
1388 reflection seismics and 2-D electrical tomopraghy. Journal of Applied Geophysics
1389 58, 144-157.
1390 Sasaki, Y., 1992. Resolution of resistivity tomography inferred from numerical
1391 simulation. Geophysical Prospecting 40, 453-464.
1392 Solá, J., Costa, J.M., 1997. Mapa Geológico de España a Escala 1:50,000, Bujaraloz
1393 (414). Instituto Tecnológico Geominero de España, Madrid.

1394 Stevenson, A., Macklin, M., Benavente, J., Navarro, C., Passmore, D., Davis, B.A.S.,
1395 1991. Cambios ambientales durante el Holoceno en el Valle del Ebro: sus
1396 implicaciones arqueológicas. Cuaternario y Geomorfología 5, 149-164.
1397 Summer, G., Homar, V., Ramis, C., 2001. Precipitation seasonality in Eastern and
1398 Southern castal Spain. International Journal of Climatology 21, 219-247.
1399 Thomas, D.S.G., 1988. The biogeomorphology of arid and semiarid environments. In:
1400 Viles, A. (Ed.), Biogeomorphology. Blackwell, Oxford, pp. 193– 221.
1401 Thorndycraft V., Benito, G., 2006. The Holocene fluvial chronology of Spain: evidence
1402 from a newly compiled radiocarbon database. Quaternary Science Reviews 25, 223-
1403 234.
1404 Utrilla, P., Rodanés, J.M., 1997. La actuación del hombre sobre el paisaje durante la
1405 Prehistoria en el Valle Medio del Ebro. In: García-Ruiz, J.M., López García, P.
1406 (Eds.), Acción humana y desertificación en ambientes mediterráneos. Instituto
1407 Pirenaico de Ecología-CSIC. Zaragoza, pp. 61-98.
1408 Valero-Garcés, B.L., Zeroual, E., Kelts, K., 1998. Arid phases in the western
1409 Mediterranean region during the last glacial cycle reconstructed from lacustrine
1410 records. In: Benito, G.; Baker, V.R.; Gregory, K.J. (Eds.). Paleohydrology and
1411 environmental Change. John Wiley and Sons, pp. 67-80.
1412 Valero-Garcés, B.L., González-Sampériz, P., Delgado-Huertas, A., Navas, A., Machín,
1413 J., Kelts, K., 2000a. Late Glacial paleohydrology and vegetational change in Salada
1414 Mediana, Central Ebro Basin, Spain. Quaternary International 73/74, 29-46.
1415 Valero-Garcés, B.L., Navas, A., Machín, J., Stevenson, T., Davis, B.A.S., 2000b.
1416 Responses of a saline ecosistem in a semi-arid region to irrigation and climate
1417 variability. The history of Salada Chiprana, Central Ebro Basin, Spain. Ambio 26,
1418 344-350.

1419 Valero-Garcés, B.L., Delgado-Huertas, A., Navas, A., Machín, J., González-Sampériz,
1420 P., Kelts, K., 2000c. Quaternary paleohydrological evolution of a playa lake: Salada
1421 Mediana, central Ebro Basin, Spain. Sedimentology 47, 1135-1156.
1422 Valero-Garcés, B.L., González-Sampériz, P., Navas, A., Machín, J., Delgado-Huertas,
1423 A., Peña-Monné, J.L., Sancho-Marcén, C., Stevenson, T., Davis, B.A.S., 2004.
1424 Paleohydrological fluctuations and steppe vegetation during the last glacial
1425 maximum in the Central Ebro valley (NE Spain). Quaternary International 122, 43-
1426 55.
1427 Van Dam, R.L., 2010. Landform characterization using geophysics: Recent advances,
1428 applications, and emerging tools. Geomorphology, 137, 57-73.
1429 Warren, J.K., 2006. Evaporites. Sediments, Resources and Hydrocarbons. Springer.
1430 Berlin, 1035 pp.
1431 Washington, R., Todd, M.C., Lizcano, G., Tegen, I., Flamant, C., Koren, I., Ginoux, P.,
1432 Engelstaedter, S., Bristow, C.S., Zender, C.S., Goudie, A.S., Warren, A., Prospero,
1433 J.M., 2006. Links between topography, wind, deflation, lakes and dust: The case of
1434 the Bodélé Depression, Chad. Geophysical Research Letters 33, L09401.
1435 Weiss, H., Courty, M.-A., Wetterstrom, W., Guichard, F., Senior, L., Meadow, R.,
1436 Curnow, A. 1993. The genesis and collapse of third millennium north
1437 Mesopotamian civilization Science 261, 995–1004.
1438 Williams, G.E., 1970. Piedmont sedimentation and late Quaternary chronology in the
1439 Biskra region of the northern Sahara. Zeitschrift für Geomorphologie,
1440 Supplementband 10, 40-63.
1441 Williams, P., 2004. Dolines. In: Gunn, J. (Ed.). Encyclopedia of Caves and Karst
1442 Science. Fitzroy Dearborn, New York, pp. 304-310.

1443 Yechieli, Y., Wood, W.W., 2002. Hydrogeologic processes in saline systems: playas,
1444 sebkhas, and saline lakes. Earth-Science Reviews 58, 343-365.
1445
1446

Table 1. Radiocarbon AMS dates for the middle La Playa terrace including label of the charcoal samples, location, laboratory and code, conventional radiocarbon ages, calibrated dates (using CALIB 6.0.1 and the data set intcal 09.14c; Reimer et al., 2009) and vertical distance from the base of the terrace deposit to the sampling point. In bold, 2 sigma calibrated age ranges used in the chronological model, with relative probabilities higher than 0.80.

Label and location	**Laboratory and code**	**Conventional radiocarbon age (yr BP)**	**Calibrated radiocarbon age (1σ)**	**Calibrated age as yr BP (2 σ)**	**Distance to base (cm)/layer number**
MT-95 Hand-dug trench	Poznan Radiocarbon Poz-39720	345±35	AD1486-1524 (0,34) AD1558-1631 (0,65)	**487-311 (1)**	405/23
MT-115 Hand-dug trench	Poznan Radiocarbon Poz-39787	2120±35	BC198-95 (1)	2299-2260 (0,07) **2158-1995 (0,92)**	385/23
BU-T-VII Backhoe trench	Poznan Radiocarbon Poz-26352	2505±35	BC767-740 (0,17) BC689-663 (0,16) BC648-549 (0,65)	**2742-2461 (0,99)** 2382-2380 (0,0006)	330/21
BU-T-V2 Backhoe trench	Poznan Radiocarbon Poz-26351	2890±35	BC1123-1013 (1)	3160-3087 (0,14) **3085-2925 (0,83)** 2904-2892 (0,01)	294/17
BU-T-IV Backhoe trench	Poznan Radiocarbon Poz-26410	3320±35	BC1635-1598 (0,36) BC1595-1531 (0,63)	**3638-3465 (1)**	256/14
BU-T-II3 Backhoe trench	Poznan Radiocarbon Poz-26348	3235±35	BC1529-1450 (1)	3557-3519 (0,13) **3512-3383 (0,86)**	221/11

BU-T2-26B Outcrop close to hand-dug trench	Beta Analytic Inc. B-230985	2980±40	BC1289-1282 (0,03) BC1269-1187 (0,64) BC1184-1153 (0,19) BC1147-1129 (0,12)	3324-3290 (0,04) **3269-3060 (0,90)** 3053-3022 (0,03) 3017-3006 (0,01)	60-99/1 based on visual correlation
BU-T2-26 Hand-dug trench	Poznan Radiocarbon Poz-21748	3520±35	BC1896-1866 (0,28) BC1849-1773 (0,71)	**3887-3699** (1)	20/1

1456

1457

1458

Sample code	Sample depth [1] (m)	Grain size (μm)	Water content [2] (%)	Beta dose rate [3, 4] (Gy/ka)	Gamma dose rate [4, 5] (Gy/ka)	Cosmic ray dose rate [6] (Gy/ka)	Total dose rate [4, 7] (Gy/ka)	Number of grains or aliquots [8]		Over-dispersion [9] (%)	D_e value [4, 10] (Gy)	OSL Age [4, 11] (ka)
UTL1	0.75	125–180	14.5	0.57 ± 0.03	0.26 ± 0.02	0.17 ± 0.02	1.04 ± 0.05	SG	133 / 900	43 ± 5	133.1 ± 6.7	127.9 ± 9.3
		90–125	14.5	0.59 ± 0.03	0.26 ± 0.02	0.17 ± 0.02	1.06 ± 0.05	MG	10 / 10	50 ± 14	134.3 ± 17.5	127.2 ± 17.9
UTL2	0.45	125–180	20.2	0.13 ± 0.02	0.10 ± 0.01	0.17 ± 0.02	0.43 ± 0.04	SG	0 / 200	-	-	-

[1] Depth below modern ground surface.

[2] Field water content, expressed as a % of dry mass of mineral fraction and assigned a relative uncertainty of ±10% to accommodate the effect of any potential variations during the burial periods.

[3] Measurements made on dried and powdered samples by low-level beta-particle counting using a Risø GM-25-5 beta counter. External beta dose rates were determined by comparing the total beta counts obtained for each sample against those obtained for a geological standard (Nussloch loess GEOPT13) having an independently determined beta dose rate. Allowance was made for the effect of grain size (Mejdahl, 1979) and HF acid etching (Brennan, 2003) on beta-dose attenuation. Beta dose rates were adjusted for moisture attenuation using present-day water contents.

[4] Mean ± total uncertainty (68% confidence interval), calculated as the quadratic sum of the random and systematic uncertainties.

[5] Calculated from *in situ* Na:TI gamma spectrometry using the energy windows approach of Aitken (1985) (see further details in Arnold et al., 2012). Gamma dose rates were derived from radionuclide concentrations of ^{40}K, ^{238}U and ^{232}Th using the published conversion factors of Adamiec and Aitken (1998) and Stokes *et al.* (2003).

[6] Determined using the approach of Prescott and Hutton (1994), adjusted for site altitude, geomagnetic latitude, and thickness and water content of sediment overburden, and assigned a relative uncertainty of ±10%.

[7] Total dose rates includes an assumed internal dose rate of 0.03 Gy / ka (Bowler *et al.,* 2003), with a relative uncertainties of ±30%.

[8] Number of single grains (SG) or multi-grain aliquots (MG) that passed the SAR rejection criteria (Arnold and Roberts, 2011; Arnold et al., 2011) and were used for D_e determination / total number of

grains or aliquots analysed.

[9] Relative standard deviation of the D_e distribution after allowing for measurement uncertainties, calculated using the central age model (CAM) of Galbraith *et al.* (1999).

[10] Final burial dose estimate, calculated using the 4-parameter minimum age model (MAM-4) of Galbraith *et al.* (1999) based on the goodness-of-fit criterion outlined by Arnold et al., (2009).

[11] Total uncertainty includes a systematic component of ±2% associated with laboratory beta-source calibration.

1459

1460 Table 2. Dose rate data, equivalent dose estimates (D_e), and OSL ages for La Playa samples.

1461

Figure captions

Figure 1. Geographic location and geological sketch of the Bujaraloz-Sástago endorheic area (modified from Salvany et al., 1996). U.D.U.: Upper Detrital Unit. M.D.U.: Middle Detrital Unit. Note that most of the closed depressions occur on the Middle Gypsum Unit, with a higher proportion of gypsum. The rectangle indicates the area covered by the geomorphological map of figure 2. Ephemeral lakes in which paleolimnological-palynilogical studies have been conducted: 1. La Playa, 2. El Pueyo, 3. El Pito, 4. La Salineta, 5. Guallar, 6. Camarón, 7. Rebollón, 8. La Clota.

Figure 2. Geomorphological map showing the distribution of terraces and yardangs in the La Playa-El Pueyo enclosed depressions. Arrows point to the trench sites in the middle terrace (MT) and the upper terrace (UT).

Figure 3. A: Desiccation cracks with salt precipitates at the edges. La Playa, May 2005. B: Blisters developed at the surface of La Playa. August 1990. C: Small pit around 30 cm across and 10 cm deep found in the bottom of La Playa, February 1989. D: Nebkhas formed at the leeside of *Salicornia sp.* and largely composed of lenticular gypsum crystals. Northeastern margin of La Playa. E: Linear dunes resulting from the coalescence of nebkha trains. Northeastern margin of La Playa, March 2002. F: Mounds of worm pellets constituting a large volume of material susceptible to deflation. La Playa, March 2001.

Figure 4. Oblique aerial view of La Playa and El Pueyo saline lakes. Arrow points to the trench sites in the middle terrace (MT) and the upper terrace (UT). In the foreground and between El Pueyo and La Playa, yardangs developed in the ESE leeside of the lake

1487 basins. Yr: Yardang developed in gypsiferous bedrock. Yls: Yardang carved in
1488 lacustrine sediments of the middle terrace.
1489
1490 Figure 5. Location, chronology, stratigraphy and main palaeoenvironmental proxies of
1491 the sedimentary sequences from La Playa and La Salineta cores (modified from
1492 González-Sampériz et al., 2008).
1493
1494 Figure 6. Orthophotograph of La Playa lake indicating the location of geophysical
1495 profiles, the trenching site at the middle terrace and position of the three boreholes
1496 carried out by previous authors with depth to bedrock. B: Installation of THE electrode
1497 array of the ERT profile T2 in the bottom of La Playa. Arrow points to hand-dug trench
1498 in the scarp of the middle terrace. C. Electrical resistivity profiles T1a, T1b, T2 and T3.
1499 Dashed lines in T1a and T3 delineate the position of the interface between different
1500 units identified in seismic refraction traverses SR1 and SR2, respectively. Average
1501 propagation P-wave velocities indicated in profiles T1a and T3.
1502
1503 Figure 7. A: Hand-dug trench excavated in the scarp of the middle terrace. B: NE wall
1504 of the backhoe trench during the sampling process. C: Backhoe trench at the edge of the
1505 terrace surface connected to the hand-dug trench by a subsidiary correlation trench.
1506
1507 Figure 8. Spatial arrangement of the trenches and logs showing the identified
1508 stratigraphic units and a correlation line between the bottom of the backhoe trench and
1509 the hand-dug trench.
1510

Figure 9. Synthetic stratigraphic log, grain size and compositional analyses (TIC, TOC and TS) of the middle terrace. The lower part (188 cm) was described in the hand-dug trench and the upper part (312 cm) in the higher quality exposure of the backhoe trench.

Figure 10. Chronological model for the middle terrace based on AMS radiocarbon ages derived from samples collected in the trenches. Age ranges represent the 2 sigma calibrated ^{14}C ranges with relative probabilities higher than 0.80. The ages that do not fit the model corresponds to a sample collected from the terrace scarp at some distance from the trenches and a sample obtained 95 cm below the terrace tread. The deviation of the lower sample is most likely related to erroneous correlation or the sampling of reworked material. The anomalous modern age of the higher sample is attributed to soil contamination.

Figure 11. A: OSL sampling position in the hand-dug trench excavated in the upper terrace. The two PVC tubes represent replicates of sample UTL1. Sample UTL2 was collected 30 cm above sample UTL1, but did not yield sufficient quartz grains for dating. B: Single-grain equivalent dose (D_e) distribution for sample UTL1, shown as a frequency histogram with ranked De estimates.

Figure 12. Geomorphic evolution of La Playa-El Pueyo lake system and graph illustrating the successive aggradation and entrenchment phases recorded by the lacustrine terraces. It is not clear whether the current lake bottom represents a strath cut-across the lower terrace or a fill inset in the latter.

Figure 13. Dated aggradation phases in ephemeral valleys within the Ebro Depression. Roman numbers correspond to relative ages based on geoarcheological criteria. Arrows and question marks indicate poorly constrained onset and/or resumption of accumulation period.

Figure 1

Click here to download high resolution image

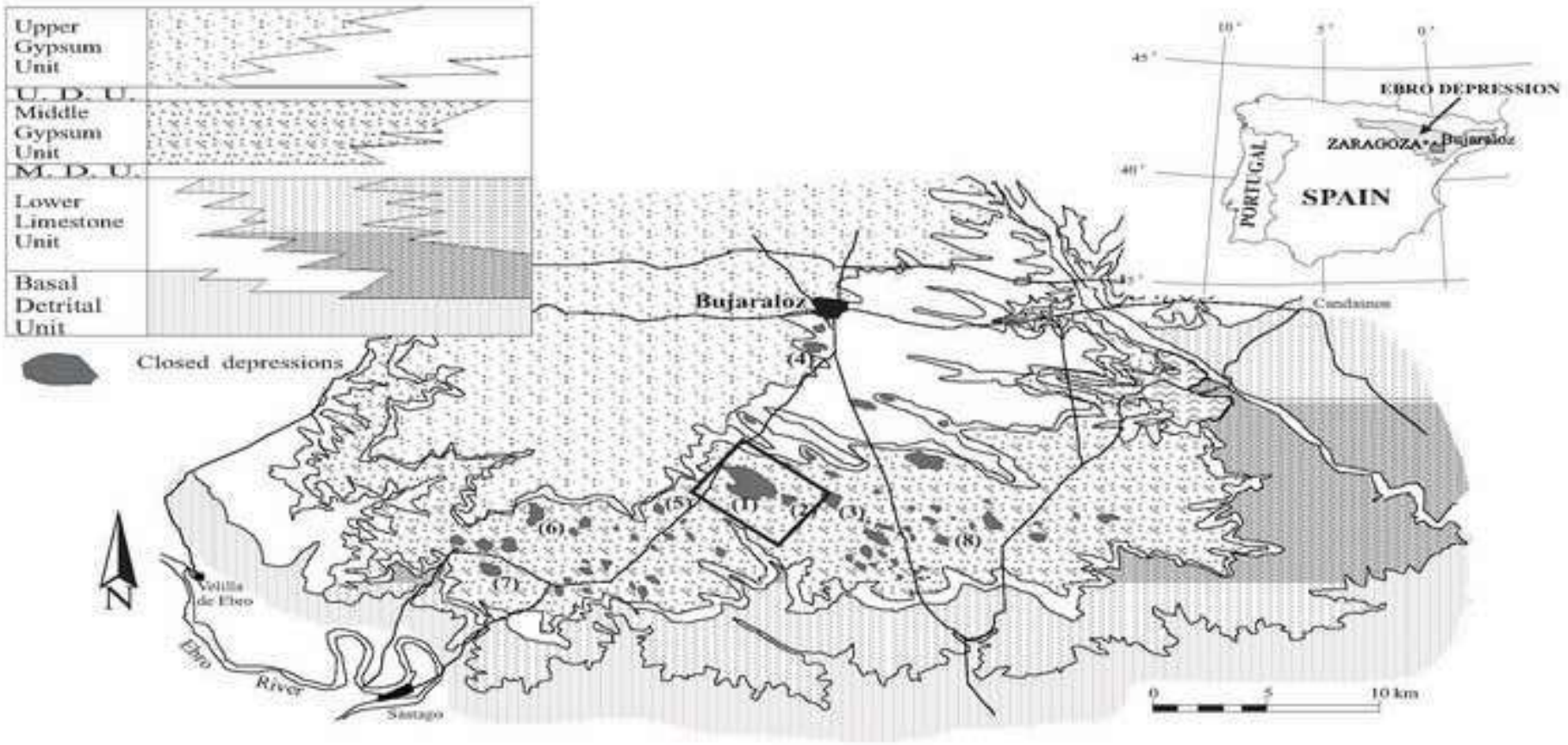

Figure 2 color

Click here to download high resolution image

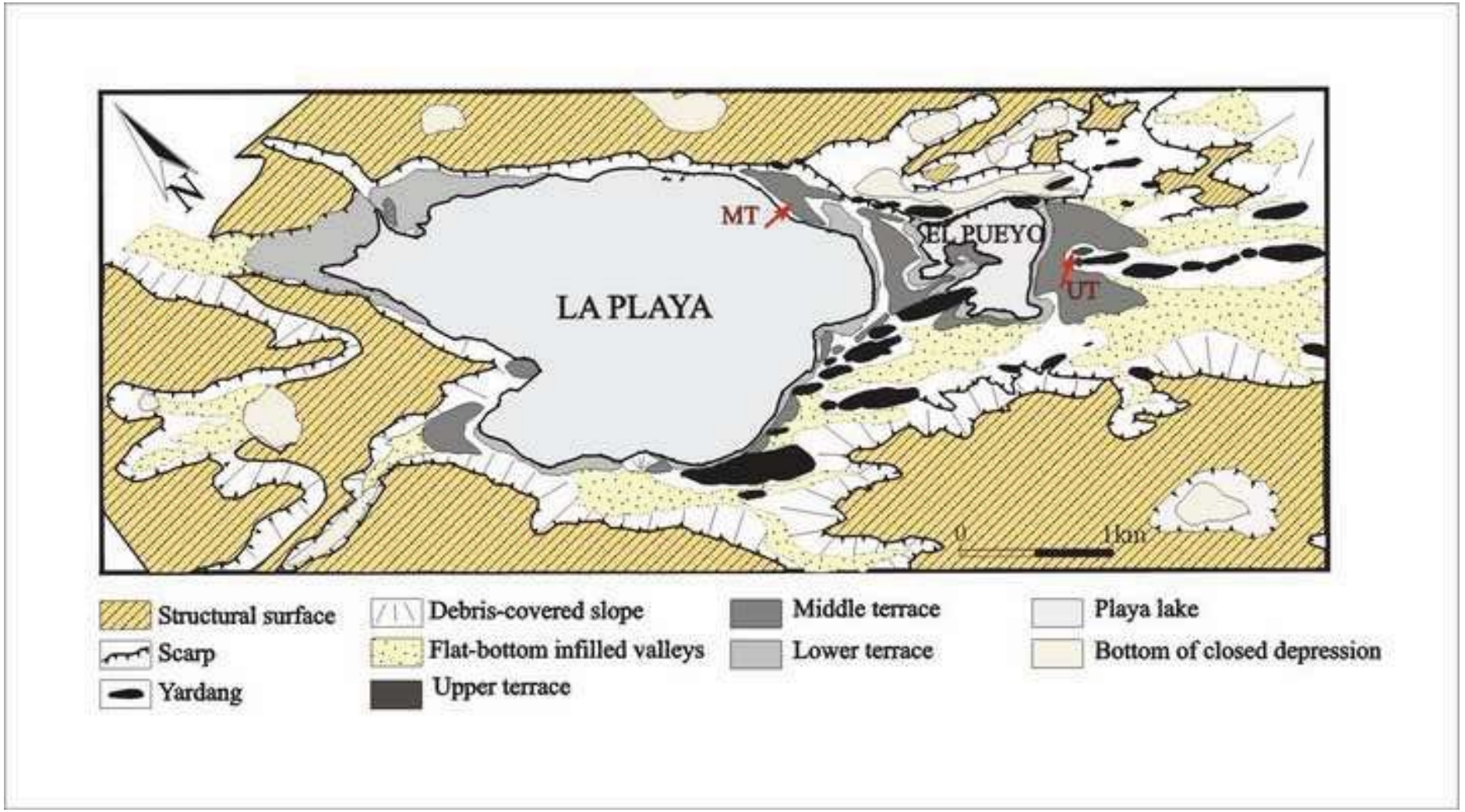

Figure 2 b&w
Click here to download high resolution image

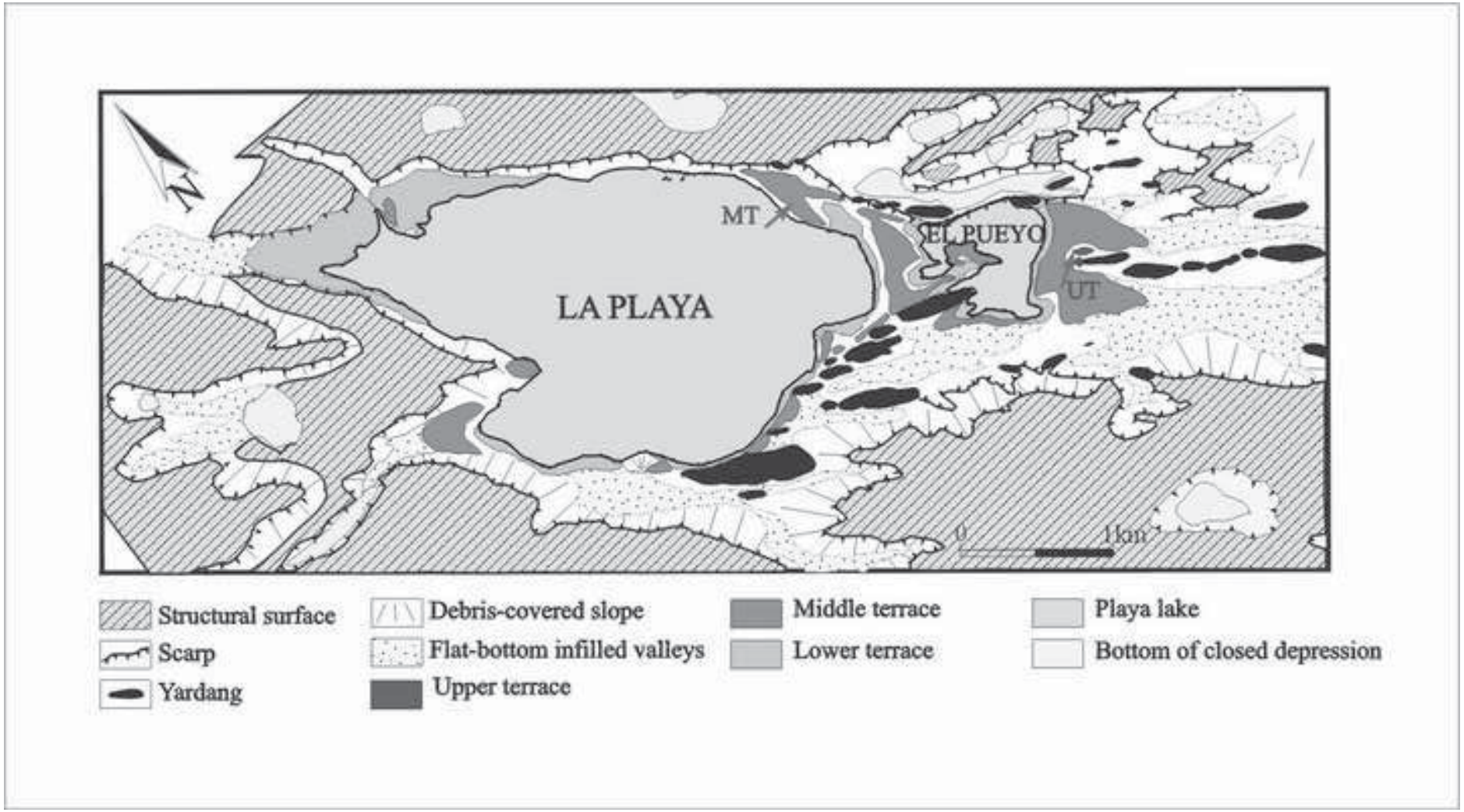

Figure 3

Click here to download high resolution image

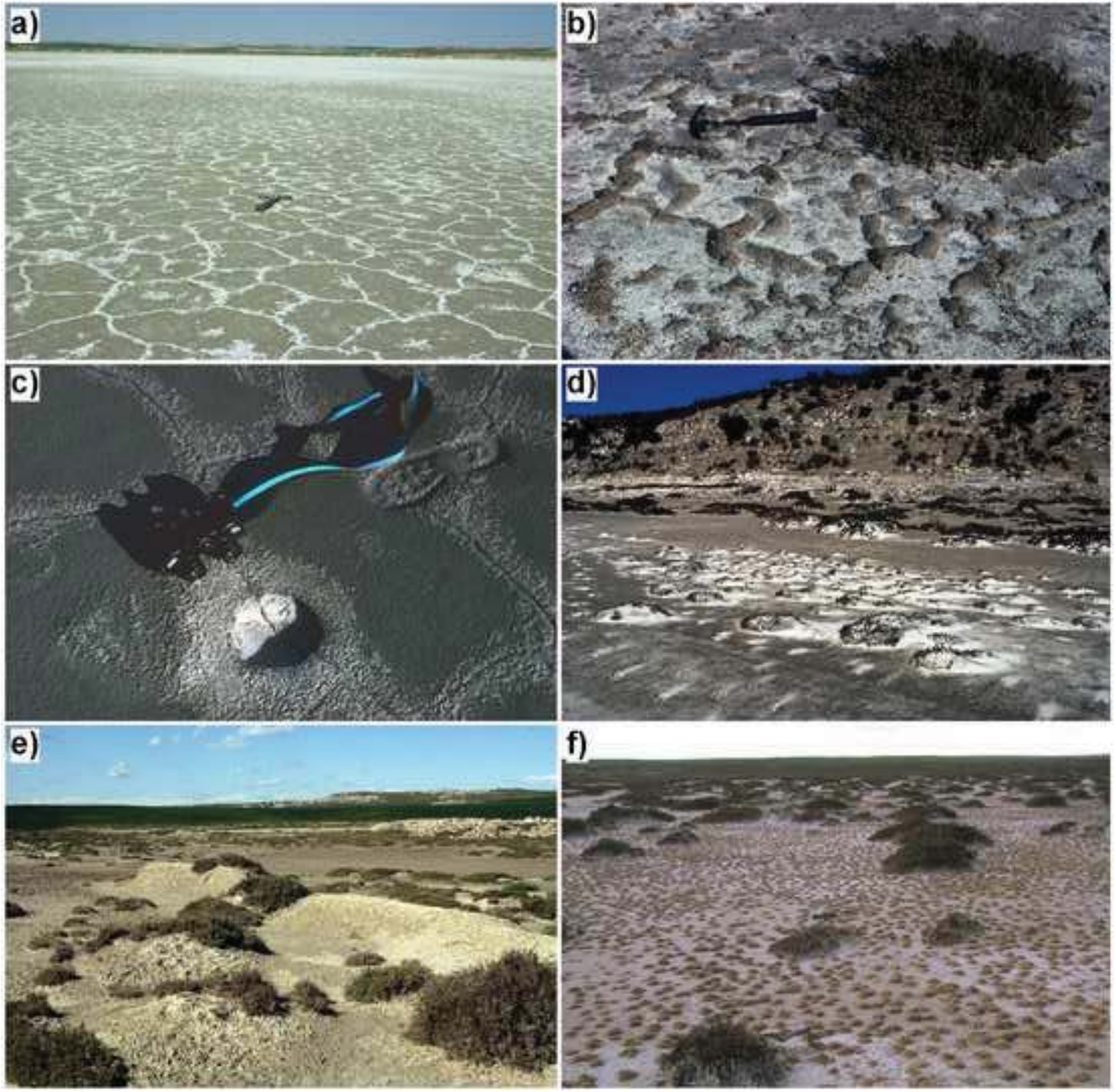

Figure 4
Click here to download high resolution image

Figure 5

Click here to download high resolution image

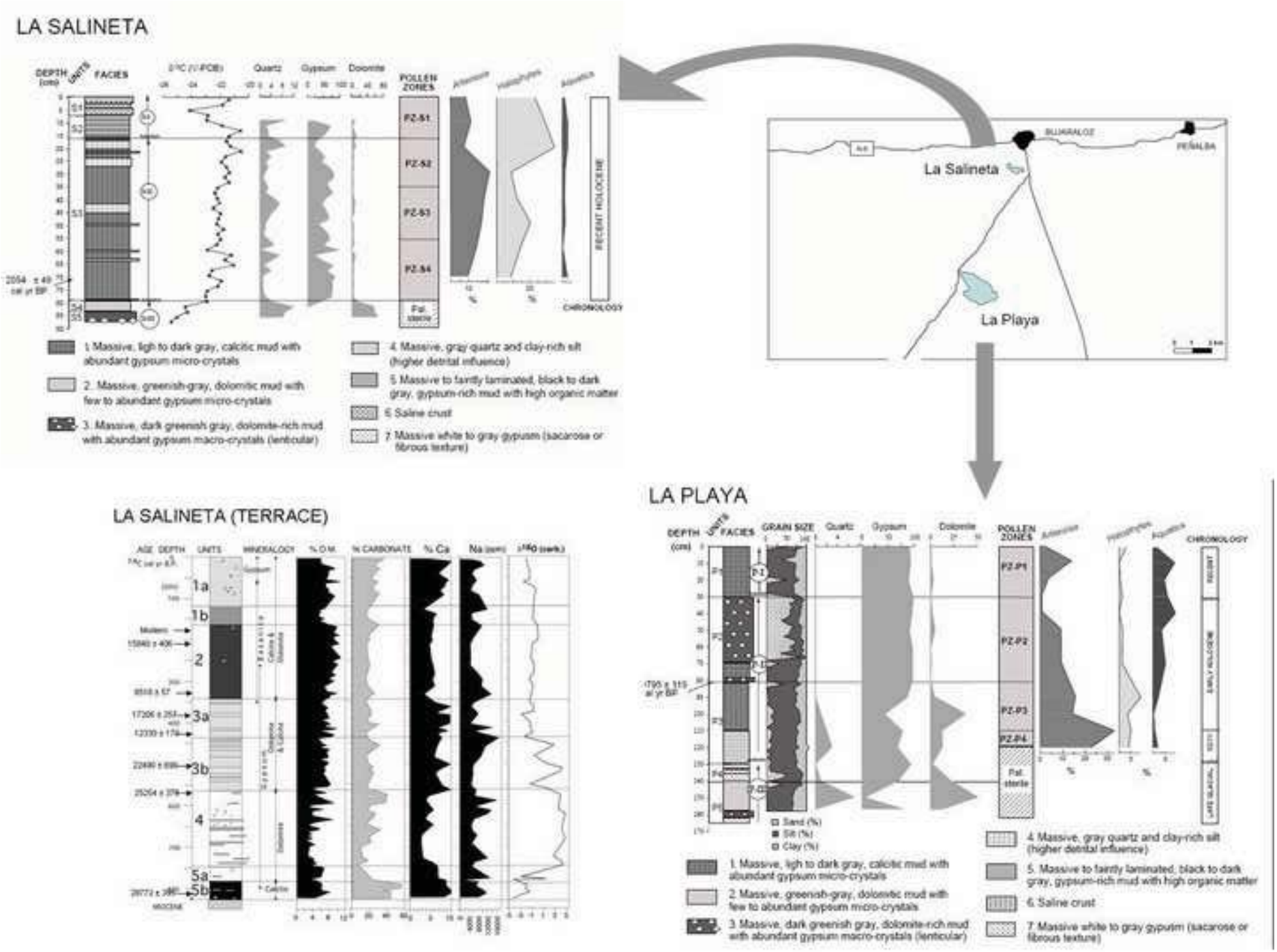

Figure 6

Click here to download high resolution image

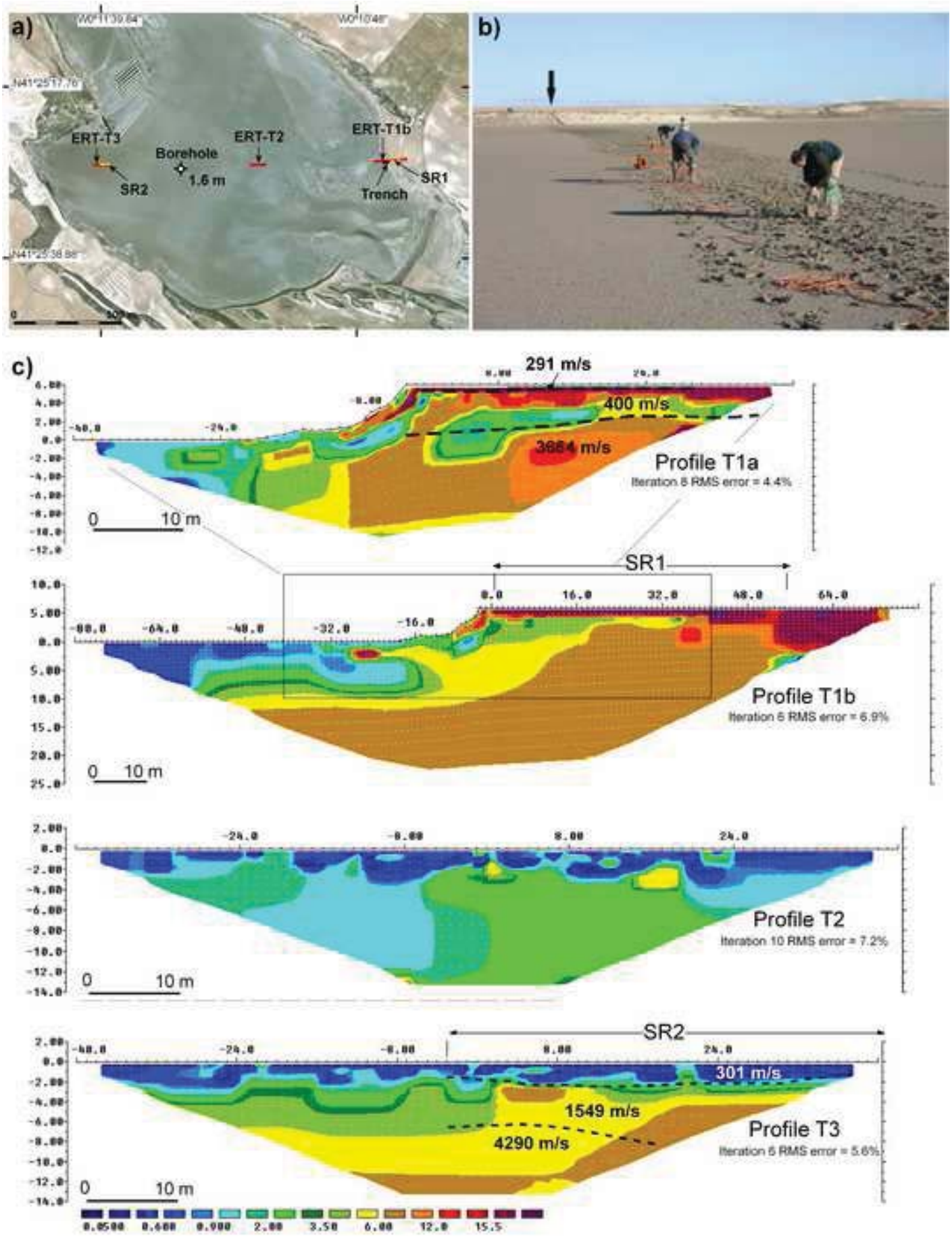

Figure 7
Click here to download high resolution image

Figure 8 color

Click here to download high resolution image

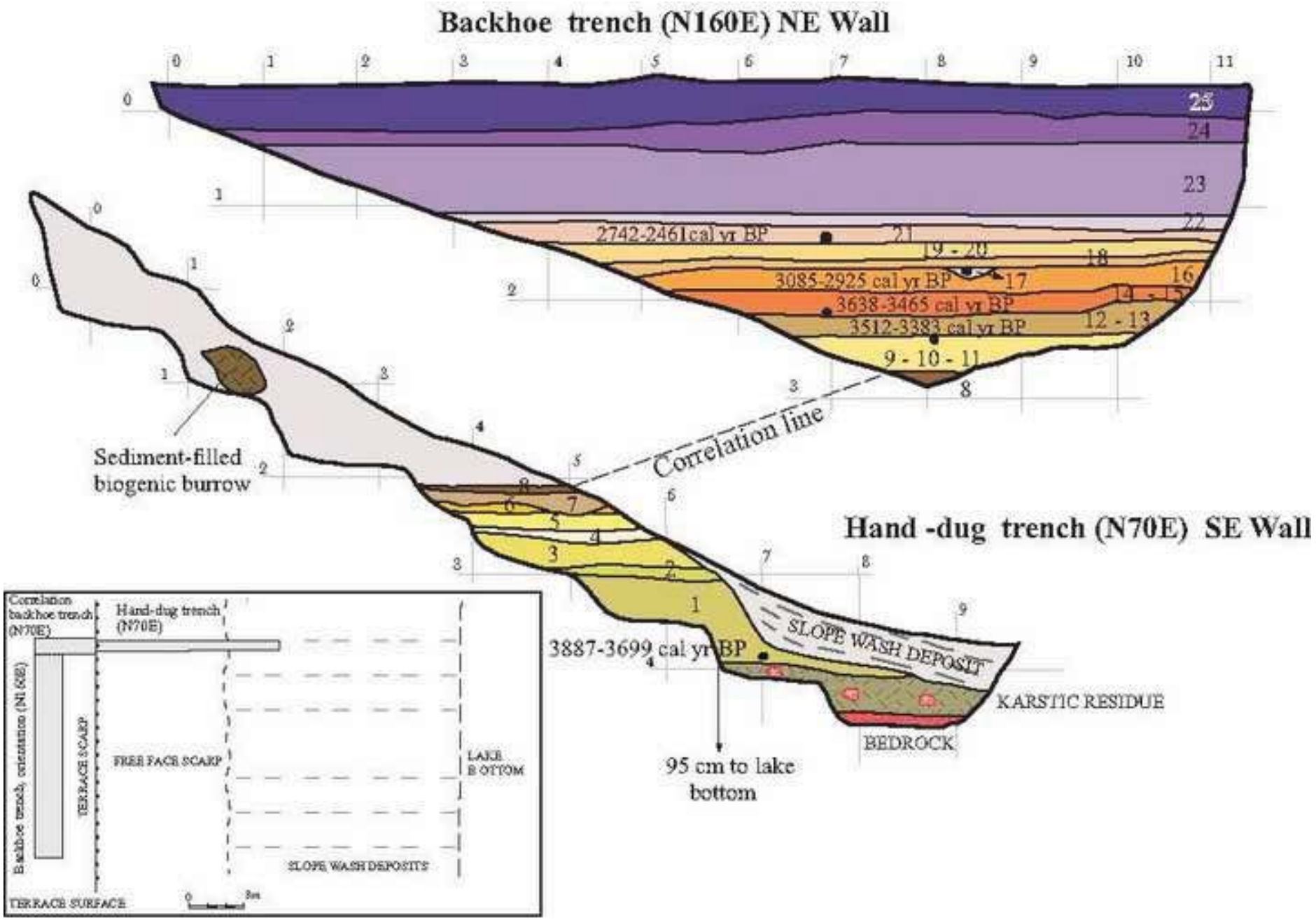

Figure 8 b&w

Click here to download high resolution image

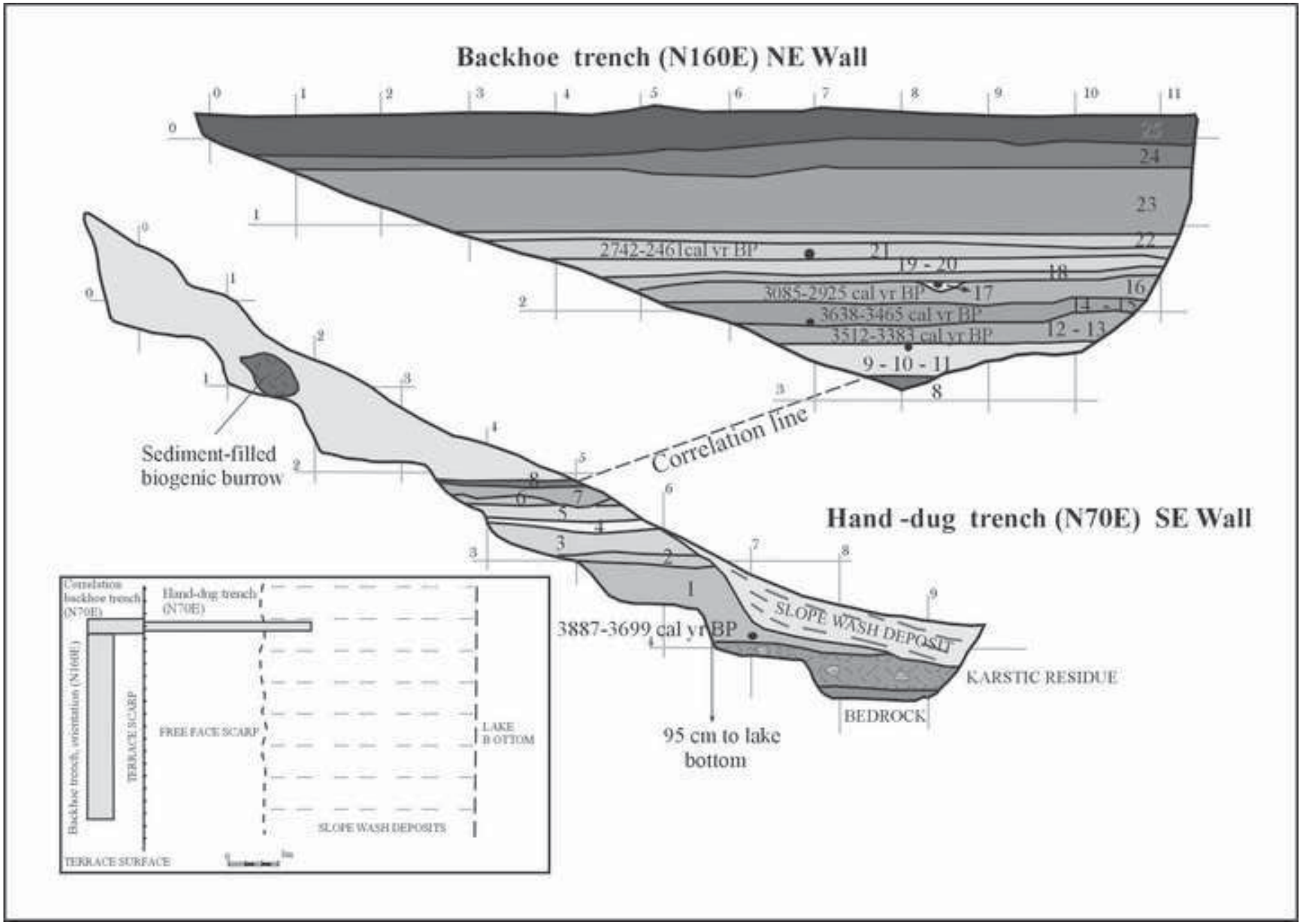

Figure 9 color

Click here to download high resolution image

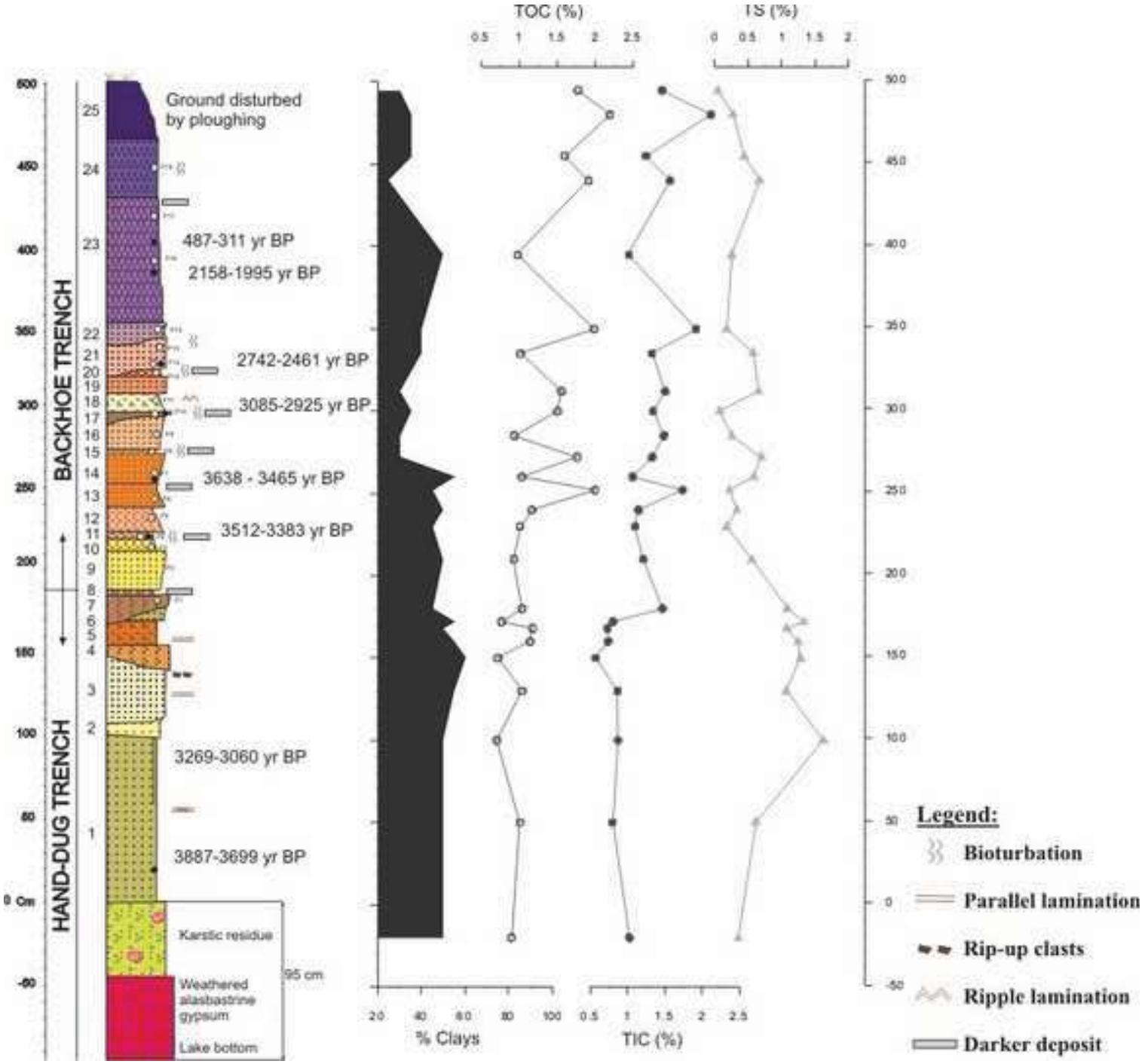

Figure 9 b&w

Click here to download high resolution image

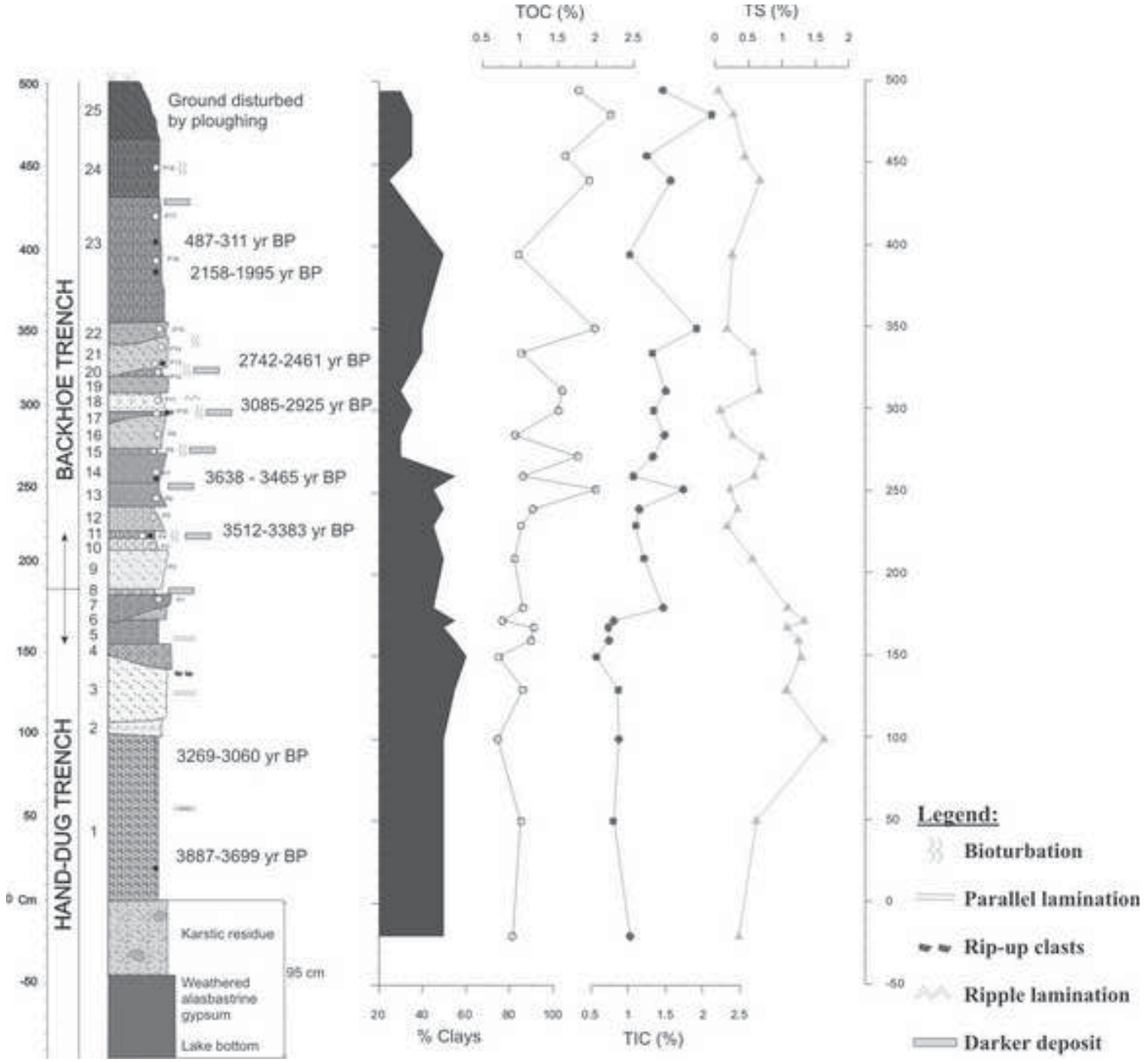

Figure 10
Click here to download high resolution image

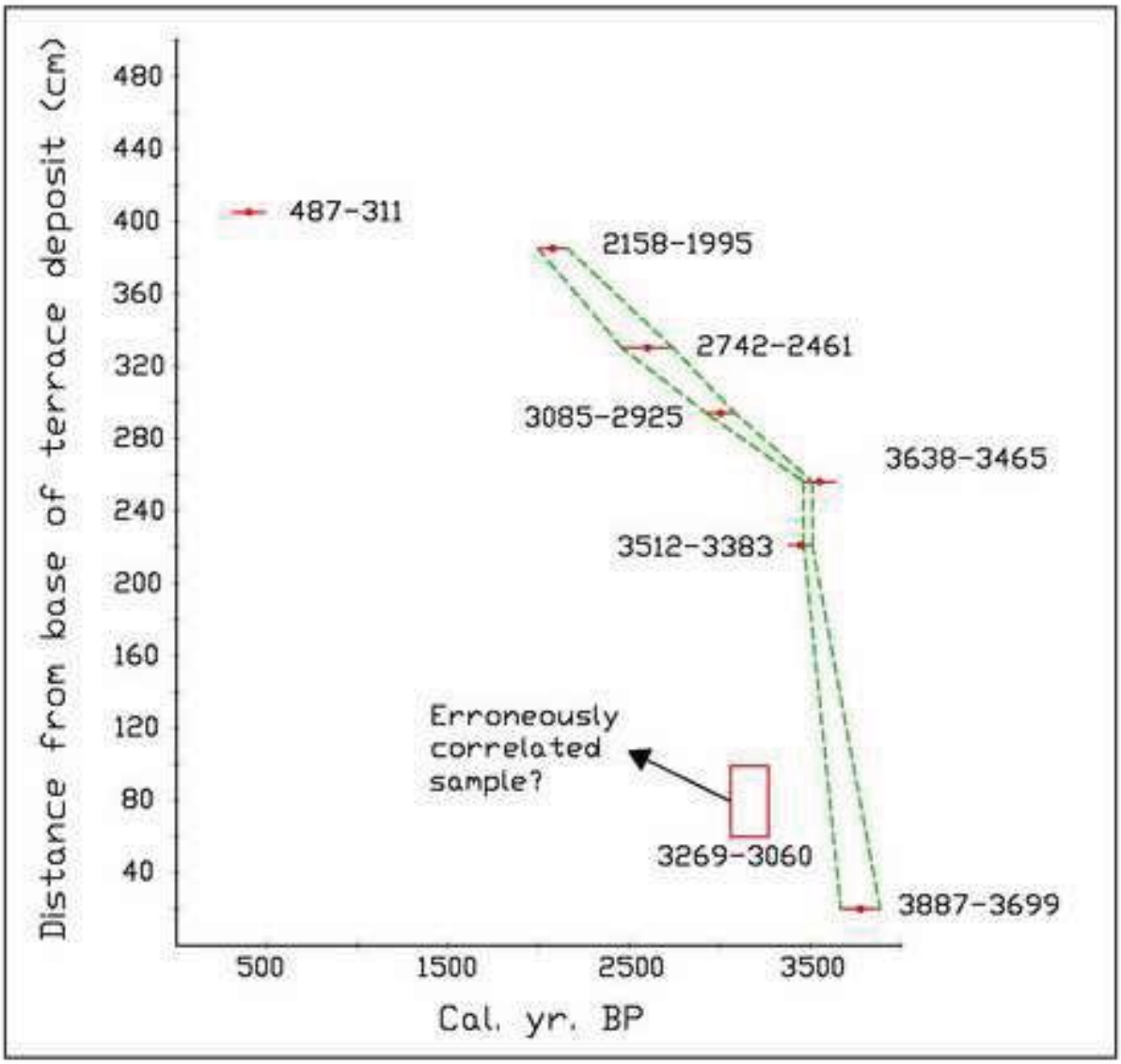

Figure 11
Click here to download high resolution image

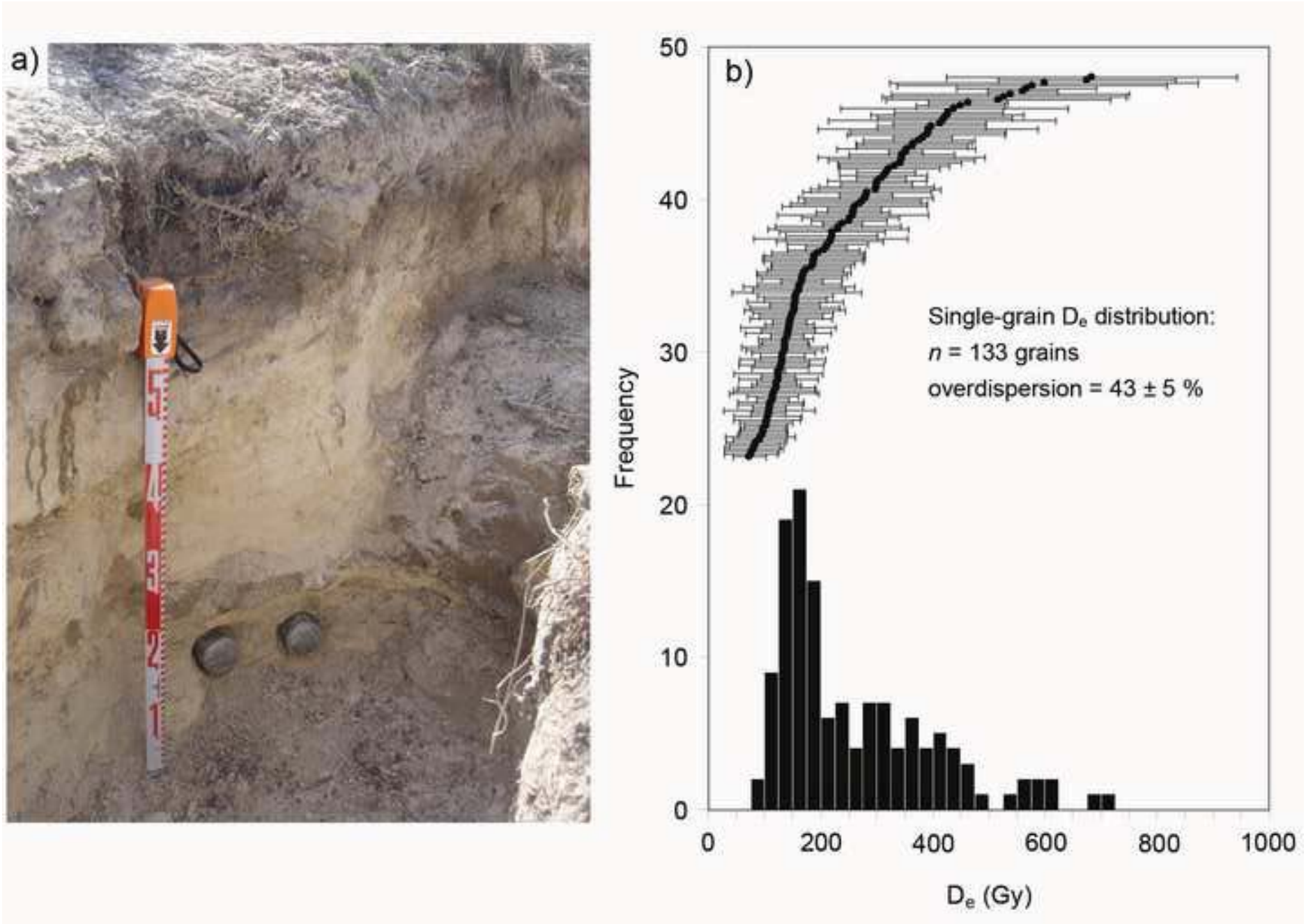

Figure 12

Click here to download high resolution image

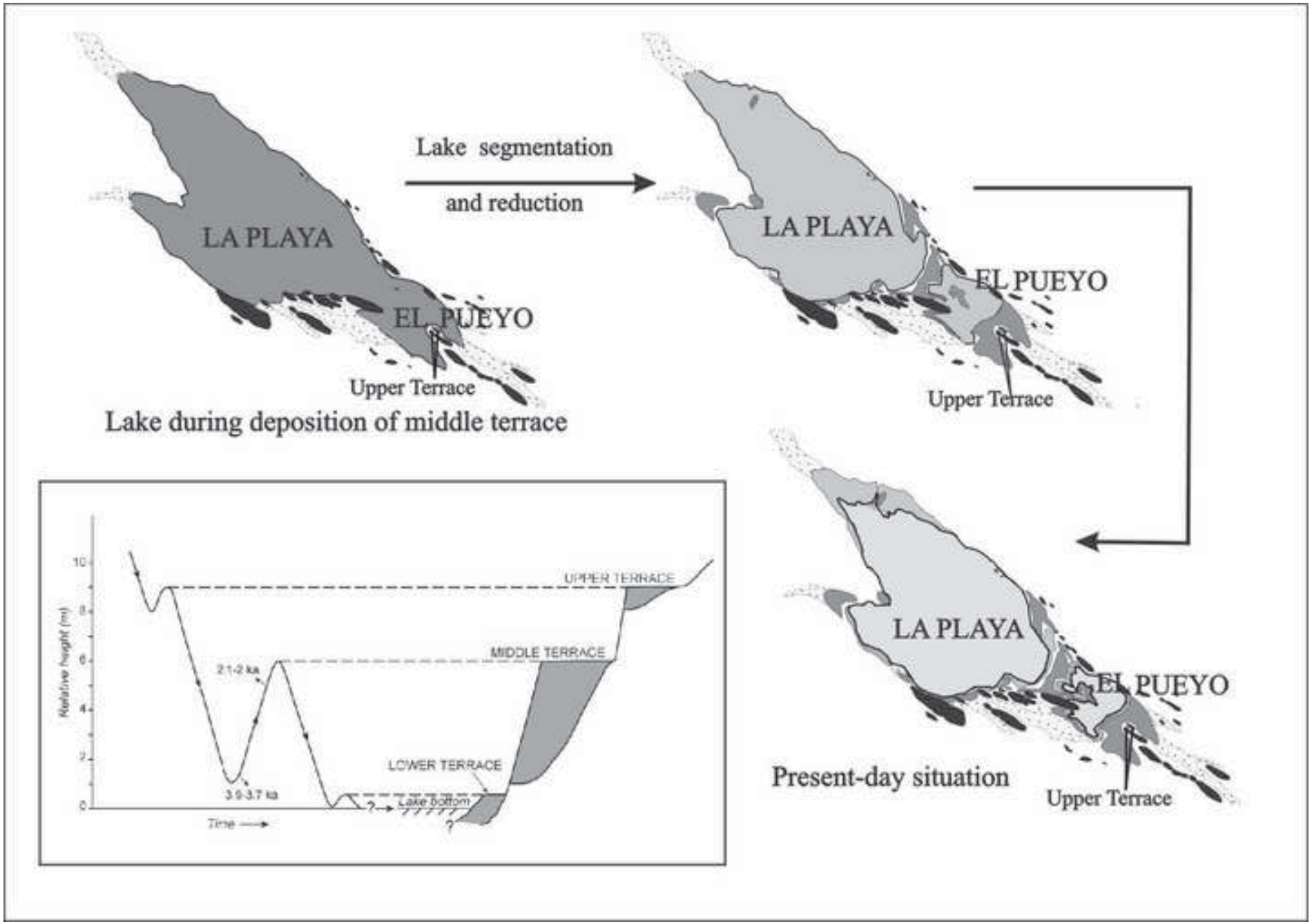

Figure 13
Click here to download high resolution image

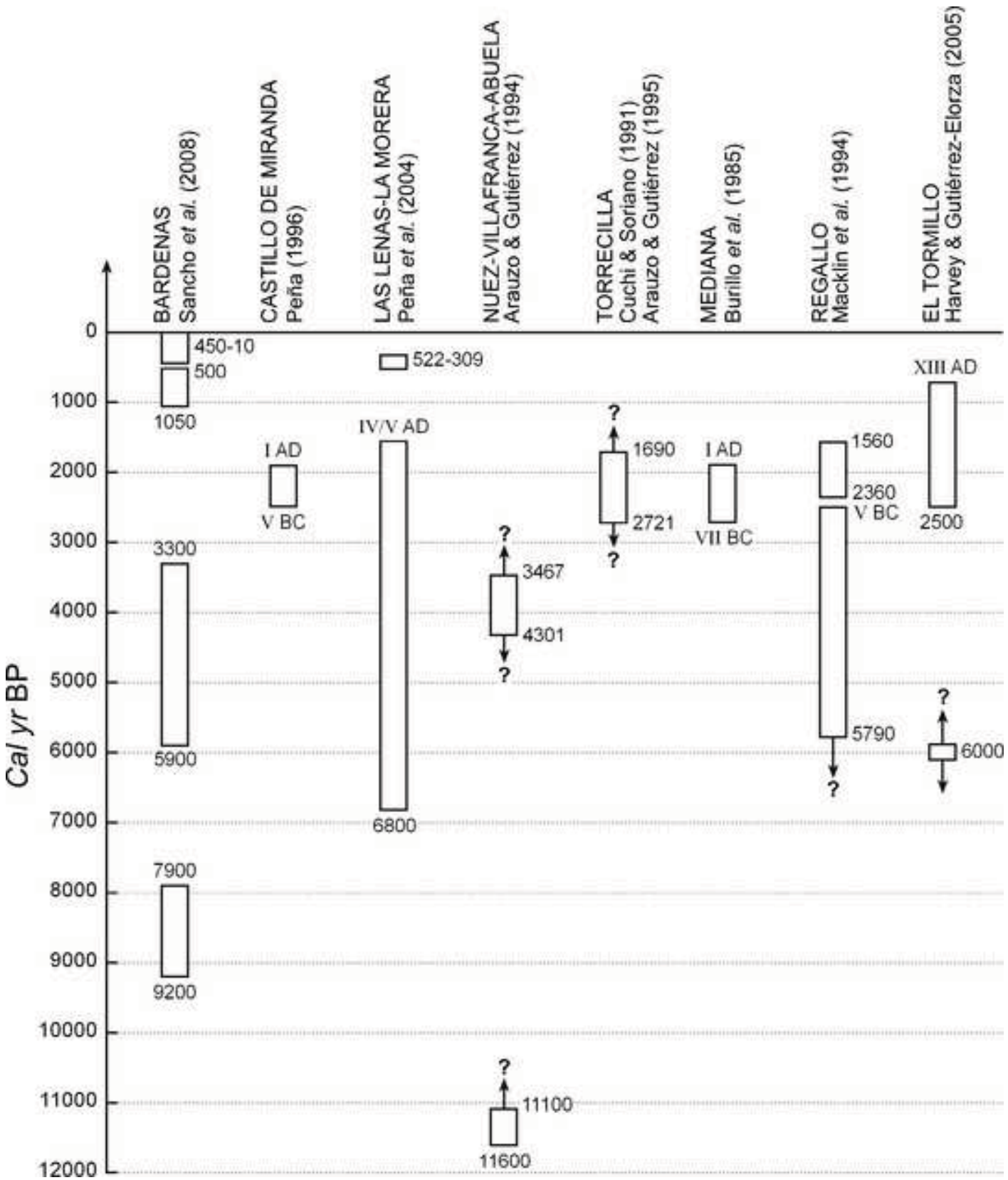

Figure 5

Click here to download high resolution image

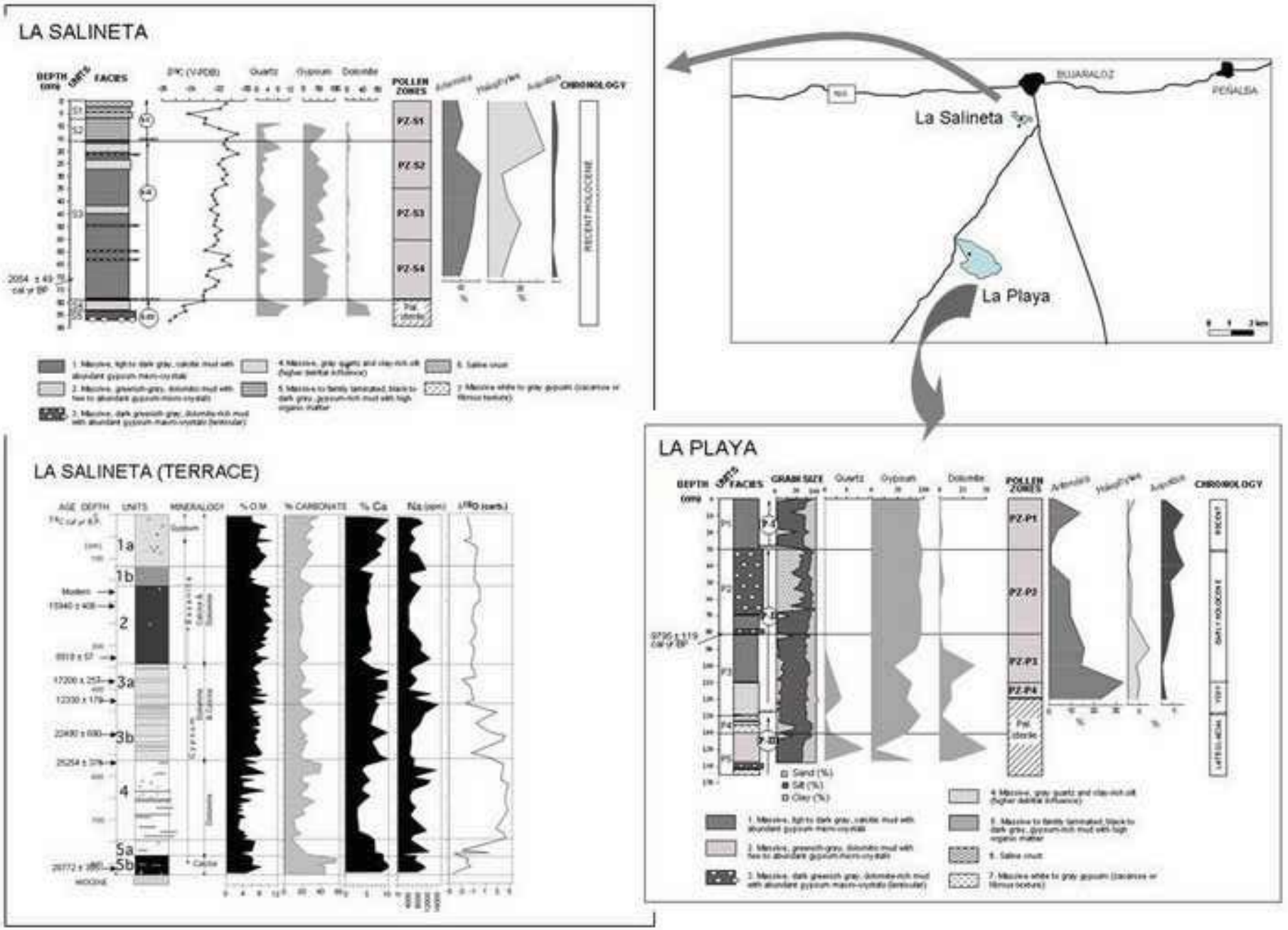

Figure 6

Click here to download high resolution image